149065

NASA CR-
_141751_

INVESTIGATIONS RELATED TO GEODETIC CONTROL ON THE MOON

Ivan I. Mueller

editor

Prepared for

National Aeronautics and Space Administration
Johnson Space Center
Houston, Texas

(NASA-CR-141751). ; INVESTIGATIONS RELATED TO   N75-72999
GEODETIC CONTROL ON THE MOON   Final Report
(Ohio State Univ. Research Foundation)
102 p   Unclas
                                           0.0/98 · 09505

The Ohio State University
Research Foundation
Columbus, Ohio   43212

February, 1973

102

Reports of the Department of Geodetic Science

Report No. 198

INVESTIGATIONS RELATED TO GEODETIC CONTROL

ON THE MOON

Ivan I. Mueller

editor

Prepared for

The Ohio State University
Research Foundation
Columbus, Ohio   43212

February, 1973

PREFACE

This project is under the supervision of Professor Ivan I. Mueller, Department of Geodetic Science at The Ohio State University, Columbus, and is under the technical direction of Mr. Richard L. Nance, Code TF 541 Mapping Sciences Branch, Earth Observation Division, NASA/JSC, Houston, Texas. The contract is administered by the Facility and Laboratory Support Branch, Code BB 631/B4, NASA/JSC, Houston, Texas.

TABLE OF CONTENTS

LIST OF TABLES

LIST OF FIGURES

1. INTRODUCTION

The main objective of this project was to design a system capable of providing geodetic information on the moon (and on the earth) consistent with the dynamics of the earth-moon system. This consistency is imperative since most modern observational systems between the earth and the moon (laser, differential VLBI, earth-based or orbital lunar photography, etc.) cannot be fully analyzed and utilized without taking into consideration all the factors which make any of them dependent on time, i.e., on dynamical factors. The most important group of factors on which the magnitude of the observations and their variations depend are the following:

Group 1. Parameters defining the position of the observation stations on the earth (or their motion) with respect to an earth-centered and earth-fixed coordinate system.

Group 2. Parameters defining the motion of the earth-centered and earth-fixed coordinate system with respect to an inertial frame of reference.

Group 3. Parameters defining the motion of the moon-center with respect to an earth-centered and inertially oriented frame of reference.

Group 4. Parameters defining the motion of a moon-centered and moon fixed coordinate system with respect to an inertial frame of reference.

Group 5. Parameters defining the lunar stations (targets) or their motions with respect to the moon-centered and moon-fixed coordinate system.

In the classical geodetic/astronomic practice, the approximate number of parameters in the above groups would be the following:

1. Earth-station parameters: 3 coordinates/station

2. Parameters defining the orientation of the earth:

    --rotational velocity   1

    --precession (Newcomb)   9

    --nutation (Woolard)   109

    --polar motion $\sim$ 50/year

3. Parameters in an analytical lunar ephemeris: $\sim$1600

4. Parameters defining the orientation of the moon (physical libration): $\sim$50

5. Lunar station parameters: 3 coordinates/station

It was clear from the beginning that it would be impractical to design a system which would attempt to correct the above several thousands of parameters simultaneously and at the same time possibly also try to recover certain systematic errors burdening the observations themselves. In order to reduce the number of unknown parameters and thereby make the approach more practical, it was decided in the beginning that the classical models for the orientations of the earth, the moon, and for the motion of the moon around the earth (groups 2 - 4 above) will each be replaced by sets of Eulerian angles and their time rates used in numerical integration procedures. Numerically integrated lunar ephemerides were already available (e.g., JPL) at that time.

Another objective of the project is to find possible improvement in the earth-moon system described above when the different types of

2

observational systems are used in various combinations with each other rather than individually, which seems to be the current practice. In the beginning it was thought that this question could be best answered in a simulated and simplified earth-moon environment where the parameters in groups 2 - 4 can be adequately computed and thus the system can be controlled at will for an extensive simulation study.

The project is not completed at the time of the termination of the present contract. It is continued under Contract No. NAS9-13093 as OSURF Project No. 3487-A1. This report attempts to summarize those individual research items which have been completed and which will be used in the attempt to reach the original goals of the project. Most items have already been reported in more detail in the interim reports listed in the Bibliography. The report is in two main sections: The first (section 2) summarizes results related to the dynamics of the earth-moon system (groups 2 - 4), such as the simulated earth-moon environment, the numerical integration of earth and moon orientation angles; the second (section 3) summarizes some preliminary results in connection with position determinations on the earth and on the moon (groups 1 and 5). Section 4 is a summary of planned future work. Credit to individual contributors is given in each section, but it must be understood that in a university environment when the researchers are mostly graduate students and their advisors, the information flow is so free and the exchange of ideas so continuous that the names at the section headings are more indicative of responsibilities and not necessarily of individual achievements, though the latter obviously should not be ruled out either.

3

2. DYNAMICS OF THE EARTH-MOON SYSTEM

2.1 Orientation of the Earth by Numerical Integration

F.A. Fajemirokun[1] and Frank Hotter

2.11 Introduction

The earth's rotational motion on its axis and its orbital revolution around the barycenter are of fundamental importance in astronomy. Both motions are complex and irregular due to the gravitational attractions of celestial bodies in the solar system, the tidal deformations of the earth, and the noncoincidence of the earth's axis of rotation with a principal axis of inertia.

The changes in the direction of the earth's instantaneous axis of rotation in an inertial space have been obtained classically by dividing the variations into two parts--namely, the secular part (precession) and the periodic part (nutation). The differential equations of motion are analytically solved by the well-known method of "variation of parameters" and, through successive approximations, and after fitting actual observations to the linearized mathematical structure, series expressions are obtained for the calculation of precessional and nutational elements. There are also variations in the angular rate of rotation (which affect the measurement and determination of time) and variations in the position of the instantaneous rotational axis within the earth (polar motion).

---

[1]Presently at the University of Lagos, Lagos, Nigeria

Presently, values of precession and nutation for any epoch calculated from the series expressions can be expected to be consistent (accuracy-wise) with present-day observation methods and instrumentation. Neverthe-less, the introduction of more precise instrumentation for future observa-tions, such as the laser and the Very Long Baseline Interferometry (VLBI), has recently reopened the possibility of more accurate determination of the parameters associated with the earth's rotational motion (such as precession, nutation and polar motion). Using these new types of observations, observa-tion equations expressing the observables as functions of parameters (which include those associated with the earth's rotation) can be used in an adjustment process to obtain corrections to existing values of the rotational parameters of the earth.

The large number of parameters involved necessitates a large number of observations over an extended period of time. The coefficients of the series expressions for nutational parameters alone number 109, while the expressions for the precessional elements contain 9 coefficients. This large number of coefficients results from the analytical methods used in solving the original equations of motion. Theoretically, the three second-order differential equations can be solved if six constants of integration are stipulated.

In this paper, a method for solving the differential equations of motion of the earth is presented. The method is based on the numerical integration. The numerical integration yields the orientation angles of a coordinate system rigidly fixed to the earth's body with respect to a fixed celestial coordinate system. The parameters associated with the earth's

5

orientation in space could thus be reduced to six initial conditions, namely, the orientation angles and their time rates at a standard epoch.

2.12 The Differential Equations of Motion of the Earth

The motion of any rigid body under the influence of external forces can be represented as the resultant of a translation, with the velocity of the center of mass, and a rotation about an axis through the center of mass. The rotational motion is determined by the moments of the external forces about the center of mass and are well treated in standard textbooks on celestial and analytical mechanics.

The force-moment equation for a rigid body can be written, according to Edwards [1964] as

$$\vec{L} = \frac{d\vec{H}}{dt} \qquad\qquad 2.1 - 1$$

where

$$\vec{L} = \sum_n \vec{r}_i \times \vec{F}_i = \text{force momentum}$$

$$\vec{H} = \sum_n m_i \vec{r}_i \times \vec{v}_i = \text{rotational momentum}$$

and

$m_i \dots m_n$ are the masses of the particles which make up the rigid body

$\vec{r}_i \dots \vec{r}_n$ are the respective position vectors of the masses of particles from the center of mass of the rigid body

$\vec{F}_i \dots \vec{F}_n$ are the external forces acting on the particles

$\vec{V}_i \dots \vec{V}_n$ are the velocities of the particles referred to the fixed origin.

For the rotating earth, let U,V,W axes represent a Cartesian coordinate system fixed to the earth's body and centered at the geocenter (for example, the 'average' terrestrial coordinate system). Further, let the X,Y,Z axes

represent an inertial coordinate system centered at the geocenter (for example, the mean ecliptic system of 1950.0). These coordinate systems are shown in Fig. 2.1-1. If OP is the instantaneous axis of rotation, coinciding with neither the W nor the Z axes, then the earth's rotational velocity can be represented by a vector W along OP. If $\vec{i}$, $\vec{j}$, $\vec{k}$ are unit vectors along the U,V,W axes respectively, then

$$\vec{\omega} = \omega_u \vec{i} + \omega_v \vec{j} + \omega_w \vec{k} \qquad 2.1 - 2$$

Since

$$\vec{v}_i = \vec{\omega} \times \vec{r}_i \qquad 2.1 - 3$$

and

$$\vec{r}_i = u\vec{i} + v\vec{j} + w\vec{k} \Rightarrow u\vec{i} + v\vec{j} + w\vec{k} \qquad 2.1 - 3$$

then

$$\vec{H} = H_u \vec{i} + H_v \vec{j} + H_w \vec{k} \qquad 2.1 - 4$$

Differentiating $\vec{H}$ with respect to time:

$$\frac{d\vec{H}}{dt} = \vec{i} \frac{dH_u}{dt} + H_u \frac{d\vec{i}}{dt} + \vec{j} \frac{dH_v}{dt} + H_v \frac{d\vec{j}}{dt} + \vec{k} \frac{dH_w}{dt} + H_w \frac{d\vec{k}}{dt} \qquad 2.1 - 5$$

From Fajemirokun [1971] the above equation can be written in matrix notation as

$$[H] = [M_I] [\omega] \Rightarrow [M_I] [\omega] \qquad 2.1 - 6$$

where

$$H = \begin{vmatrix} H_u \\ H_v \\ H_w \end{vmatrix}, \qquad M_I = \begin{vmatrix} A & -F & -E \\ -F & B & -D \\ -E & -D & C \end{vmatrix}, \qquad \omega = \begin{vmatrix} \omega_u \\ \omega_v \\ \omega_w \end{vmatrix}$$

and

A,B,C,D,E,F are the six constants of inertia as defined in Edwards [1964].

Thus

7

$$\frac{d\vec{H}}{dt} = M_I \dot{\vec{\omega}} + \vec{\omega} \times \vec{H} \qquad\qquad 2.1 - 7$$

If $\vec{V}$ represents the total potential energy of a system of n bodies of finite dimensions acting on the earth, and $\vec{X}_1$, $\vec{X}_2$, ... $\vec{X}_n$ are the vectors from the geocenter to the centers of the bodies, then the force moment $\vec{L}$ is given as [Fajemirokun, 1971]:

$$\vec{L} = d\vec{V}_1 \times \vec{X}_1 + d\vec{V}_2 \times \vec{X}_2 + ... + d\vec{V}_n \times \vec{X}_n \qquad\qquad 2.1 - 8$$

where

$$d\vec{V}_i = -\frac{3GM_i}{R^5_i} [M_I \vec{X}_i]$$

G   is the gravitational constant,

M_i is the mass of body i,

R_i is the distance of body i from the geocenter.

Consequently,

$$\vec{L} = -3G\left[\frac{M_1}{R^5_1} M_I\vec{X}_1 \times \vec{X}_1 + \frac{M_2}{R^5_2} M_I\vec{X}_2 \times \vec{X}_2 + ... + \frac{M_n}{R^5_n} M_I\vec{X}_n \times \vec{X}_n\right] \quad 2.1 - 9$$

Equating equations 2.1 - 7 and 2.1 - 9,

$$M_I\dot{\vec{\omega}} + \vec{\omega} \times M_I\vec{\omega} = -3G\left[\frac{M_1}{R^5_1} M_I\vec{X}_1 \times \vec{X}_1 + ... + \frac{M_n}{R^5_n} M_I\vec{X}_n \times \vec{X}_n\right] \qquad 2.1 - 10$$

which is the unsimplified dynamic equations of motion of the earth (rotational), assuming the earth is a rigid body. Equation 2.1 - 10 reduces to the well-known Euler's equations of motion [Plummer, 1960] if it is further assumed that the products of inertia (D, E, F) are zero.

Through equation 2.1 - 10, the earth's rotational motion is represented as a   rotation about an axis which constantly passes through its center of mass,

but whose position within the earth and its direction in space varies from instant to instant. A geometrical equation can also be obtained by defining two coordinate systems, one fixed in space and the other fixed to the earth's body. Then the motion of the earth-fixed coordinate system with respect to the space-fixed system could be expressed mathematically.

The orientation of the earth in space at any instant can be defined as usual by the three Eulerian angles [Edwards, 1964; Woolard, 1953] θ, ψ and Φ. These angles are shown in Fig. 2.1-1. From the figure, the following geometrical relationships follow:

$$\left.\begin{array}{l} \omega_u = - \dot\theta \cos \Phi - \dot\psi \sin \theta \sin \Phi \\ \omega_v = - \dot\theta \sin \Phi - \dot\psi \sin \theta \cos \Phi \\ \omega_w = \dot\psi \cos \theta + \dot\Phi \end{array}\right\} \qquad 2.1 - 11$$

or, in vector notation

$$\vec\omega = S_1 \vec{\dot E} \qquad\qquad 2.1 - 12$$

where

$$S_1 = \begin{vmatrix} - \cos \Phi & - \sin \theta \sin \Phi & 0 \\ - \sin \Phi & \sin \theta \cos \Phi & 0 \\ 0 & \cos \theta & 1 \end{vmatrix}, \quad \dot E = \begin{vmatrix} \dot\theta \\ \dot\psi \\ \dot\Phi \end{vmatrix}, \quad \omega = \begin{vmatrix} \omega_u \\ \omega_v \\ \omega_w \end{vmatrix}.$$

The differentiation of equation 2.1 - 12 with respect to time gives

$$\vec{\dot\omega} = S_1 \vec{\ddot E} + \dot S_1 \vec{\dot E} = S_1 \vec{\ddot E} + S_2 E_2 \qquad 2.1 - 13$$

where

$$S_2 = \begin{vmatrix} -\cos \theta \sin \Phi & \sin \Phi & -\sin \theta \cos \Phi \\ -\cos \theta \cos \Phi & \cos \Phi & \sin \theta \sin \Phi \\ -\sin \theta & 0 & 0 \end{vmatrix}; \quad E_2 = \begin{vmatrix} \dot\theta\,\dot\psi \\ \dot\theta\,\dot\Phi \\ \dot\psi\,\dot\Phi \end{vmatrix}$$

P — Instantaneous Pole

ω — Earth's Rotational Velocity

XYZ — Mean Ecliptic (1950.0) Coordinate System

UVW — Average Terrestial Coordinate System

θ ψ Φ — Eulerian Angles

Fig. 2.1-1   The fundamental coordinate systems and the Eulerian angles.

Equation 2.1 - 13 expresses the earth's rotational motion geometrically in terms of the Eulerian angles and their time rates. Substituting these geometrical equations into the dynamical equations 2.1 - 10 and retaining $\ddot{E}$ on the left-hand side, we obtain:

10

$$\ddot{\vec{E}} = [M_I S_1]^{-1} \left\{ -3G \left[\frac{M_1}{R_1^5} M_I \vec{X}_1 \times \vec{X}_1 + \ldots + \frac{M_n}{R_n^5} M_I \vec{X}_n \times \vec{X}_n \right] - M_I S_2 \dot{\vec{E}}_2 + M_I S_1 \dot{\vec{E}} \times S_1 \dot{\vec{E}} \right\}$$

2.1 - 14

The above equation is a system of three second-order differential equations of motion, and the solution for $\vec{E}$ (the Eulerian angles) gives the orientation of the earth in space at any desired epoch.

2.13 Numerical Integration of the Differential Equations of Motion

In previous analytical solutions of the earth's differential equations of motion [Woolard, 1953], the earth's products of inertia (D, E, F) are assumed to be zero, and it is also assumed that the earth possesses rotational symmetry about the W-axis (i.e., A = B). Furthermore, the external forces acting on the earth are limited to those produced by the sun and the moon.

In this study, the moment of inertia (M_I) matrix is taken to be a full one, and A is not necessarily equal to B. Also, in addition to the sun and moon, four other planets are used as sources of external forces in equation 2.1 - 14. These planets are Mercury, Venus, Mars and Jupiter. The three second-order differential equations of motion (equation 2.1 - 14) are transformed into a form suitable for numerical integration by setting

$$Y = \begin{vmatrix} E \\ \dot{E} \end{vmatrix}$$

so that

$$\dot{Y} = \begin{vmatrix} \dot{E} \\ \ddot{E} \end{vmatrix} = \begin{vmatrix} \dot{E} \\ f(E,\dot{E}) \end{vmatrix}$$

2.1 - 15

which represents a system of six first-order differential equations. These equations can be numerically integrated by any available numerical

11

integration algorithm, based on any standard numerical integration method. The method used in this study is the variable-order Adams predictor-corrector method, developed and used by the Jet Propulsion Laboratory (JPL) in their Orbital Determination Programs. A description of the integration algorithm and its special advantages are contained in [Krogh, 1969].

In order to obtain the earth's orientation angles at a given epoch t, the six first-order differential equations of motion (represented by equation 2.1 - 15) are numerically integrated from a starting epoch t_0. The six constants of integration are the starting values:

$$Y_{t_0} = \begin{vmatrix} E \\ \dot{E}E \end{vmatrix}_{t_0} = \begin{vmatrix} \theta_0 \\ \psi_0 \\ \Phi_0 \\ \dot{\theta}_0 \\ \dot{\psi}_0 \\ \dot{\Phi}_0 \end{vmatrix}$$

which may also be referred to as the initial conditions. θ_0, ψ_0 and Φ_0 are calculated (for epoch t_0) using equations derived in Fajemirokun [1971], and their time rates are obtained through numerical differentiation. Also, in order to numerically integrate equation 2.1 - 15, $\ddot{\vec{E}}$ must be evaluated from equation 2.1 - 14. $\ddot{\vec{E}}$ is dependent on certain parameters in addition to the values of θ, ψ, and Φ. These parameters include the earth's moment of inertia matrix, the gravitational constants of the six celestial bodies, and the geocentric position of these celestial bodies.

Using the coefficients of spherical harmonics taken from Rapp [1969], the moment of inertia matrix used in these studies is:

$$M_I = \frac{1}{K} \begin{vmatrix} 0.32967 & -0.1692 \times 10^{-5} & 0 \\ -0.1692 \times 10 & 0.32968 & 0 \\ 0 & 0 & 0.33076 \end{vmatrix}$$

12

·where

$$K = \frac{1}{Ma_e^2}$$

a_e, M are the earth's semi-major axis and mass respectively. The geocentric position of the sun, moon and the four planets were taken from the JPL Development Ephemeris 69 (DE-69) tape [O'Handley et al., 1969] which is obtained through numerical integration and is believed to be gravitationally consistent. The planetary masses used are from the JPL system of planetary masses [Melbourne et al., 1968] and Table 2.1-1 gives the gravitational constant for each astronomical body.

Table 2.1-1

Gravitational Constants

Body	Gravitational Constants (Km^3/day^{-2})
Earth	0.2975542×10^{16}
Moon	0.3659906×10^{14}
Sun	0.9906936×10^{21}
Mercury	0.1655848×10^{15}
Venus	0.2425068×10^{16}
Mars	0.3197127×10^{16}
Jupiter	0.9458682×10^{18}

The values obtained for the integrated angles and their time rates at any desired epoch depends, to some extent, on values chosen for the initial conditions and the parameters of integration (e.g., inertia matrix, gravitational constants, etc.). It is therefore necessary to provide a means through which the estimated values of the initial condition and other parameters can be corrected in an adjustment process involving some form of observation. Such a procedure is described in Fajemirokun [1971] and utilizes

13

state transition and parameter sensitivity matrices. The matrix of partial

derivatives

$$U = \begin{vmatrix} \dfrac{\partial E}{\partial E_0} & \dfrac{\partial E}{\partial \dot{E}_0} \\ \dfrac{\partial \dot{E}}{\partial E_0} & \dfrac{\partial \dot{E}}{\partial \dot{E}_0} \end{vmatrix}$$

is the state transition matrix, while the parameter sensitivity matrix is

given by

$$V = \begin{vmatrix} \dfrac{\partial E}{\partial \alpha} \\ \dfrac{\partial \dot{E}}{\partial \alpha} \end{vmatrix}$$

where α represents the list of parameters.

2.14 Numerical Experiments and Results

In the previous sections of this study, it has been proposed to calcu-

late the earth's orientation in space by numerically integrating the rota-

tional differential equations of motion of the earth. The equations of

motion were derived with only one assumption--that of the earth's rigidity.

Such a new practical approach to an old problem as proposed here demands

some confirmation as to the validity of the method numerically, and some

verification of the correctness of the derived equations. Consequently,

some numerical experiments were performed mainly to verify the equations,

the computer programs and the procedure for adjusting the initial conditions.

An important aid in verifying the computer programs was the Simulated

Earth-Moon Environment Data (hereafter referred to as the simulated data)

which was created by Papo [1971]. The generated data consists of the

geocentric position and velocity of the moon, the orientation angles of

the earth and the moon and their time rates, the state transition matrices

of both the earth and the moon and their parameter sensitivity matrices.
These quantities were obtained by numerical integration of equations based
on a moderately complex model of the earth-moon dynamic system consisting
of a rotationally symmetric rigid earth and a perfectly rigid moon whose
dynamic shape is that of a triaxial ellipsoid. Other details of the mathe-
matical formulation of the equations of motion of this simplified earth-
moon system are contained in the work of Papo [1971].

A simulated ephemeris of the earth and the moon was created for a
period of one year beginning at 2440222.5 JD (1969.0). The ephemeris
contains numerically integrated geocentric positions and velocities of
the moon and the Eulerian angles and their time rates for the earth and
the moon, recorded at half-day intervals. In addition, a fifth-order
modified Everett interpolation formula [O'Handley et al., 1969] was avail-
able for use in interpolating the quantities at epochs which fall between
tabulated values.

The following two groups of numerical experiments are reported in this
section:

(a) Fitting the numerically integrated earth's Eulerian angles to those
    obtained from the simulated data.

(b) Comparing the numerically integrated Eulerian angles of the earth to
    their counterparts obtained through classical methods.

2.141 Fitting the Numerically Integrated Eulerian Angles to
       Simulated Angles.

This experiment was performed in order to provide an independent check
on the equations of motion of the earth as developed in this study and the
computer programs based on them. Since the simulated data was used, the

computer program written for the real case was slightly modified to accommodate the following restrictions imposed by the simulated environment model:

(1) In the moment of inertia matrix, A = B, and D = E = F = 0.

(2) Only the moon is the external celestial body whose potential affects the rotation of the earth.

(3) The geocentric position of the selenocenter at any epoch is that given by the simulated data rather than that obtainable from a real lunar ephemeris.

The equations of motion were integrated using the DVDQ subroutine [Krogh, 1969].

A comparison of integrated angles with their counterparts from the simulated data shows differences which were less than $0''0001$ for θ and $0''001$ for ψ and ϕ over the one year period. These results indicate perfect agreement between the two numerical integration programs (one for this study and the other used in creating the simulated data) as well as the equations on which the computer programs were based.

The adjustment program and the ability of the adjustment method to recover the initial conditions were also tested numerically. For this purpose, the theoretical initial conditions (i.e., values of the integrated quantities at the initial epoch of 2440222.5 JD), read from the simulated data, were varied. Three test runs were made in which

(1) only the initial angles were varied,

(2) both the initial angles and their time rates were varied,

(3) only the time rates of the angles were varied.

The adjustment was performed over an interval of forty days beginning at

16

2440222.5 JD and ending at 2440262.5 JD. Values of the angles integrated with wrong initial conditions were compared with the "true" values at half daily intervals. Table 2.1-2 shows the "correct" initial conditions and the initial conditions used in each of the three cases listed above.

Table 2.1-2

Starting Initial Conditions for Three Test Cases

Symbol	Correct Initial Values	Initial Values for Case 1	Initial Values for Case 2	Initial Values for Case 3
θ	0.4091596226	0.4091693189	0.4091644707	0.4091596226
ψ	-0.131898×10^{-5}	-0.110152×10^{-4}	-0.616711×10^{-5}	-0.131898×10^{-5}
Φ	4.8950936587	4.8951033498	4.8950985068	4.8950936587
$\dot{\theta}$	0.659363×10^{-7}	0.659363×10^{-7}	0.725299×10^{-7}	0.725299×10^{-7}
$\dot{\psi}$	-0.300932×10^{-5}	-0.30093×10^{-5}	-0.303942×10^{-5}	-0.303942×10^{-5}
$\dot{\Phi}$	6.3003883741	6.3003883741	6.3003943826	6.3003943826

$(\theta, \psi, \Phi$ in radians, $\dot{\theta}, \dot{\psi}, \dot{\Phi}$ in rad/day)

Table 2.1-3 presents the adjusted values of the initial conditions for the three cases after two iterations. Comparison of the recovered parameters with their "correct" values shows agreement up to the ninth decimal places (equivalent to 0".0002 for the angles and 0".0002/day for their time rates). The residuals obtained after the adjustment (by comparing integrated angles with counterparts from the simulated data) were, for all three angles and in all three cases, less than 0".0001 throughout the adjustment interval. Figs. 2.1-2 and 2.1-3 show the residuals after adjustment for the most general case (case 2).

17

Table 2.1-3

Recovered Initial Conditions for Three Test

Cases After Two Iterations

Symbol	Correct Initial Values	Recovered Initial Values for Case 1	Recovered Initial Values for Case 2	Recovered Initial Values for Case 3
θ	0.4091596226	0.4091596227	0.4091596227	0.4091596226
ψ	-0.131898×10^{5}	-0.131869×10^{5}	-0.131880×10^{5}	-0.131860×10^{5}
Φ	4.8950936587	4.8950936584	4.8950936585	4.8950936584
$\dot{\theta}$	0.659363×10^{7}	0.652045×10^{7}	0.654780×10^{7}	0.649609×10^{7}
$\dot{\psi}$	-0.300932×10^{6}	-0.298465×10^{6}	-0.299432×10^{6}	-0.300307×10^{6}
$\dot{\Phi}$	6.3003883741	6.3003883718	6.3003883727	6.3003883735

(θ, ψ, Φ in radians, $\dot{\theta}$, $\dot{\psi}$, $\dot{\Phi}$ in rad/day)

As can be seen from Table 2.1-4 which presents the correlation matrix, a few of the parameters in the solution have poor separation from others. In particular, there is a strong correlation between $\dot{\psi}$ and $\dot{\Phi}$ and moderately high correlation between $\dot{\theta}$ and ψ. In spite of these high correlations, the result of this experiment shows that in the adjustment performed, the

Table 2.1-4

Correlation Matrix for Adjusted Initial Values

in the Simulated Case

	θ	ψ	Φ	$\dot{\theta}$	$\dot{\psi}$	$\dot{\Phi}$
θ	1.00					
ψ	-0.17	1.00				
Φ	0.10	-0.35	1.00			
$\dot{\theta}$	0.22	-0.76	0.46	1.00		
$\dot{\psi}$	0.41	-0.41	0.25	0.54	1.00	
$\dot{\Phi}$	-0.41	0.41	-0.26	-0.54	-0.99	1.00

Fig. 2.1-2   Residuals in θ and ψ before and after adjustment
(simulated case).

Residuals in Φ Before Adjustment

Residuals in Φ After Adjustment

60″

40″

20″

0″

JD 2440222.5   227.5   232.5   237.5   242.5   247.5   252.5   257.5   262.5
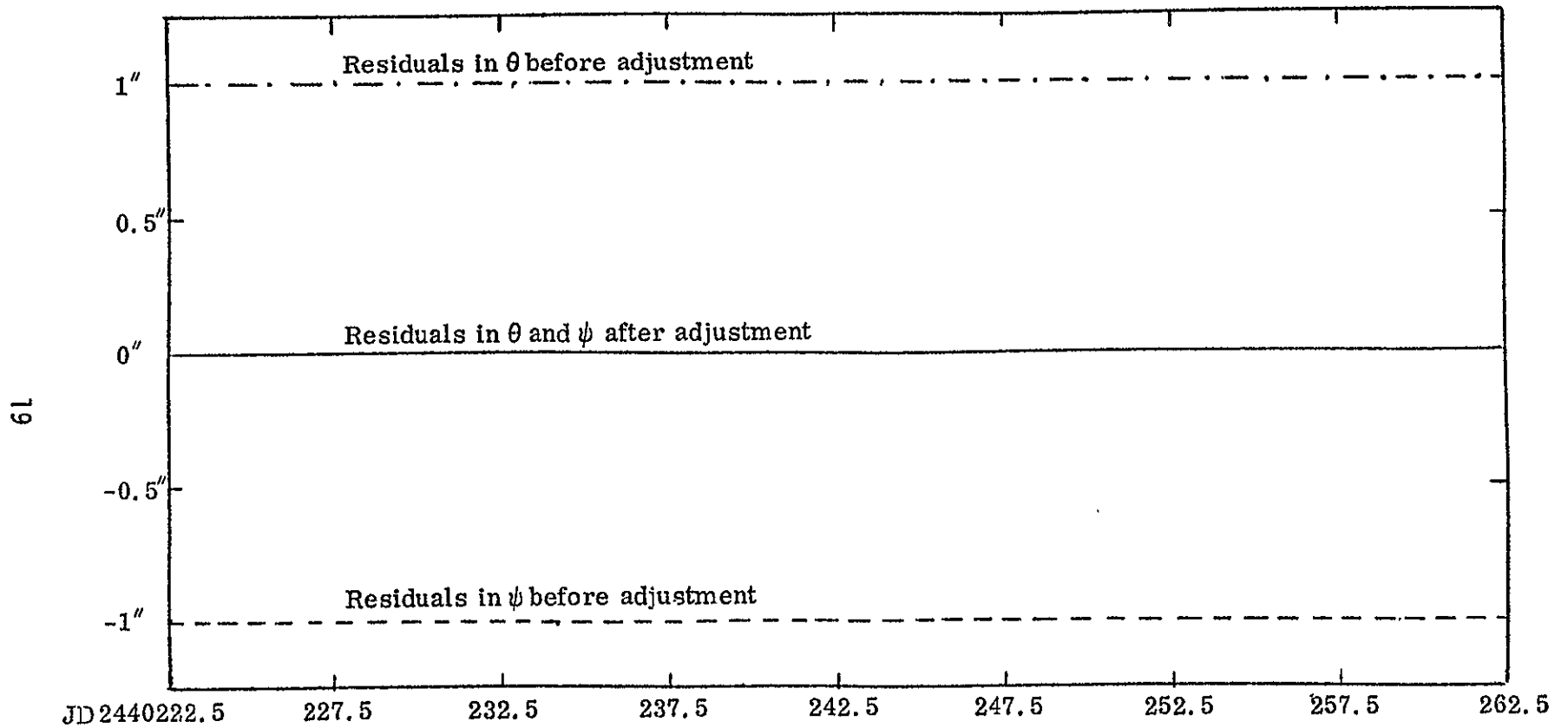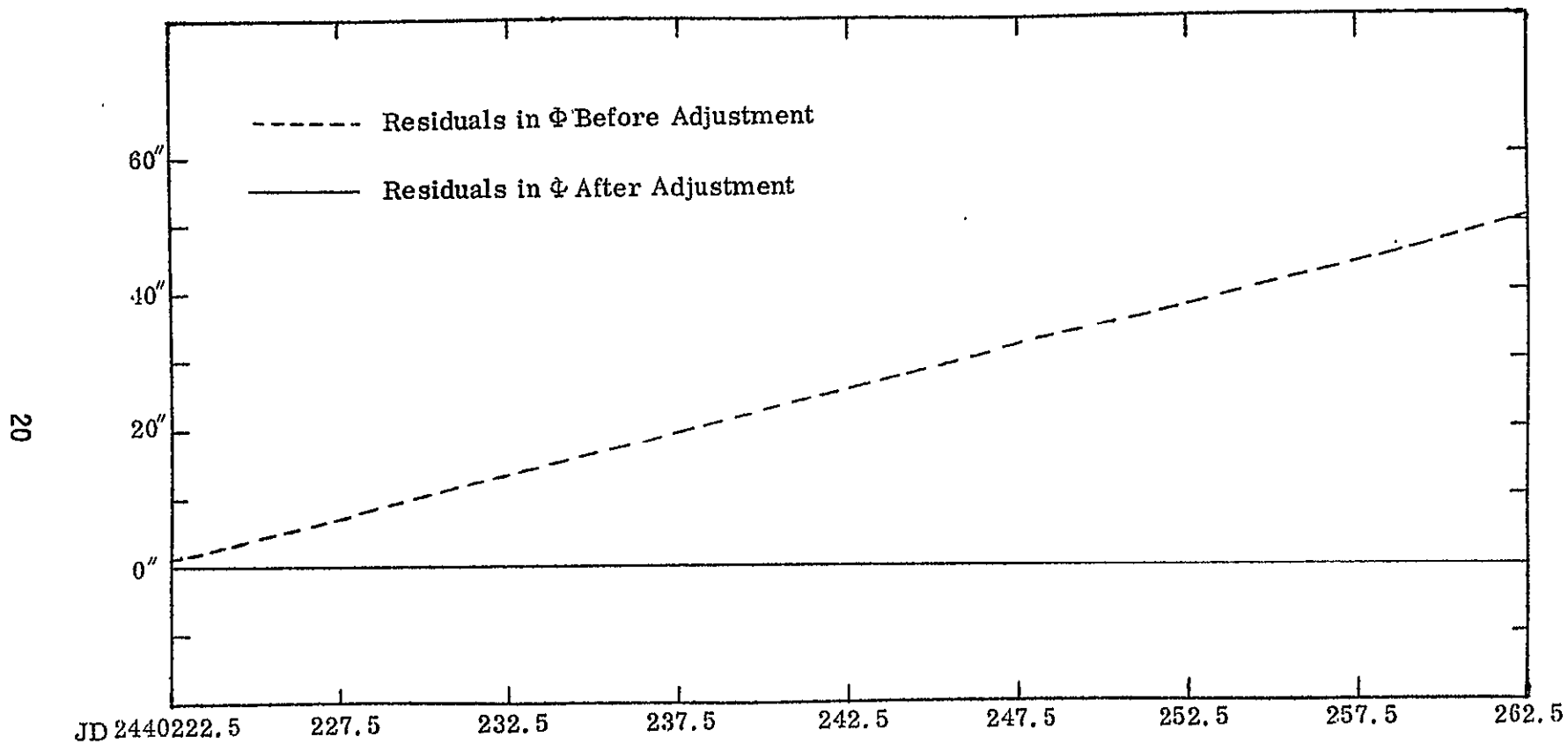
Fig. 2.1-3   Residuals in Φ before and after adjustment
(simulated case).

solution for all the parameters actually converges to their true values. This particular adjustment performed over forty days with only two iterations took approximately five minutes to run on an IBM 360/75 computer.

2.142 Comparison of Numerically Integrated Eulerian Angles with Classical Reductions.

In order to further test the numerical theory, experiments were conducted to compare the integrated Eulerian angles with similar angles computed from classical theory. Three problems became evident:

(1) First, the integrated angles refer to the body axis of the fictitious solid earth. Hence, to compare with classical precession nutation theory, it is necessary to refer the angles to the rotation axis. If we define the rotations to the rotation axis by

$$\alpha = \tan^{-1} \left[\frac{\omega_1}{\omega_3} \right]$$

$$\beta = \tan^{-1} \left[\frac{\omega_2}{\omega_3} \right]$$

2.1 - 16

where ω_1, ω_2, ω_3 refer to ω_u, ω_v, ω_z given by equation 2.1 - 11. The observed celestial coordinate system is then given in terms of the Eulerian angles by

$$\left| \begin{matrix} X \\ Y \\ Z \end{matrix} \right|_{OBS} = R_1(-\beta)R_2(\alpha)R_3(\phi)R_1(-\theta)R_3(\psi) \left| \begin{matrix} X \\ Y \\ Z \end{matrix} \right|_{1950.0}$$

2.1 - 17

Correspondingly, the same coordinates are given through classical reduction procedures using the Greenwich Apparent Sidereal Time (GAST), the precession and nutation matrices (P, N) and the obliquity of the ecliptic (ε_0) at the epoch 1950.0 as [Mueller, 1969]

$$\left| \begin{matrix} X \\ Y \\ Z \end{matrix} \right|_{OBS} = R_3(GAST) \ N \ P \ R_1(-\varepsilon_0) \left| \begin{matrix} X \\ Y \\ Z \end{matrix} \right|_{1950.0}$$

2.1 - 18

21

In order to compare the two theories, it was assumed that the 3×3 matrix products from equations 2.1 - 17 and 2.1 - 18 were composed of three angles between the mean ecliptic system of 1950.0 and the observed system as

$$R_3(\overline{\phi})R_1(-\overline{\theta})R_3(\overline{\psi}) = R_3(GAST)N \ P \ R_1(-\varepsilon_0)$$
$$R_3(\overline{\overline{\phi}})R_1(-\overline{\overline{\theta}})R_3(\overline{\overline{\psi}}) = R_1(-\beta)R_2(\alpha)R_3(\phi)R_1(-\theta)R_3(\psi)$$

2.1 - 19

Then the differences between the angles were minimized by least squares theory to adjust the desired initial state vector and/or parameters in the numerical theory.

(2) Second, the gravitational constants and moment of inertia ratio (C - A)/C in the conventional theory are defined by the constant of nutation of 9″210 at 1900 and the constant of general precession in longitude 5025″64 per tropical century at 1900 [Woolard, 1953, p. 124]. Therefore, to make the comparison realistic these values were used in the numerical integration and as in Woolard's theory the principal moments A and B were assumed to be equal, with nondiagonal elements (D, E, F) assumed to be zero.

(3) The third difficulty arose from assuming A = B and D = E = F = 0. From equation 2.1 - 10 it can be shown that

$$\dot{\omega}_3 = 0$$

or

$$\omega_3 = constant = k$$

2.1 - 20

Hence, from equation 2.1 - 11 we have

$$\omega_3 = k = \dot{\psi} \cos \theta + \dot{\phi}$$

2.1 - 21

Therefore, if we "set" an initial state vector defining $\dot{\psi}$, θ, and $\dot{\phi}$, the constant is determined and we would expect $\dot{\psi}$, $\dot{\phi}$ to be highly correlated as shown in Fig. 2.1-4. To overcome this problem $\dot{\phi}$ was assumed to be dependent on $\dot{\psi}$ and only the values θ, ψ, ϕ, $\dot{\psi}$ in the state vector were adjusted. Further, it was assumed that over the period of integration t_0 to t:
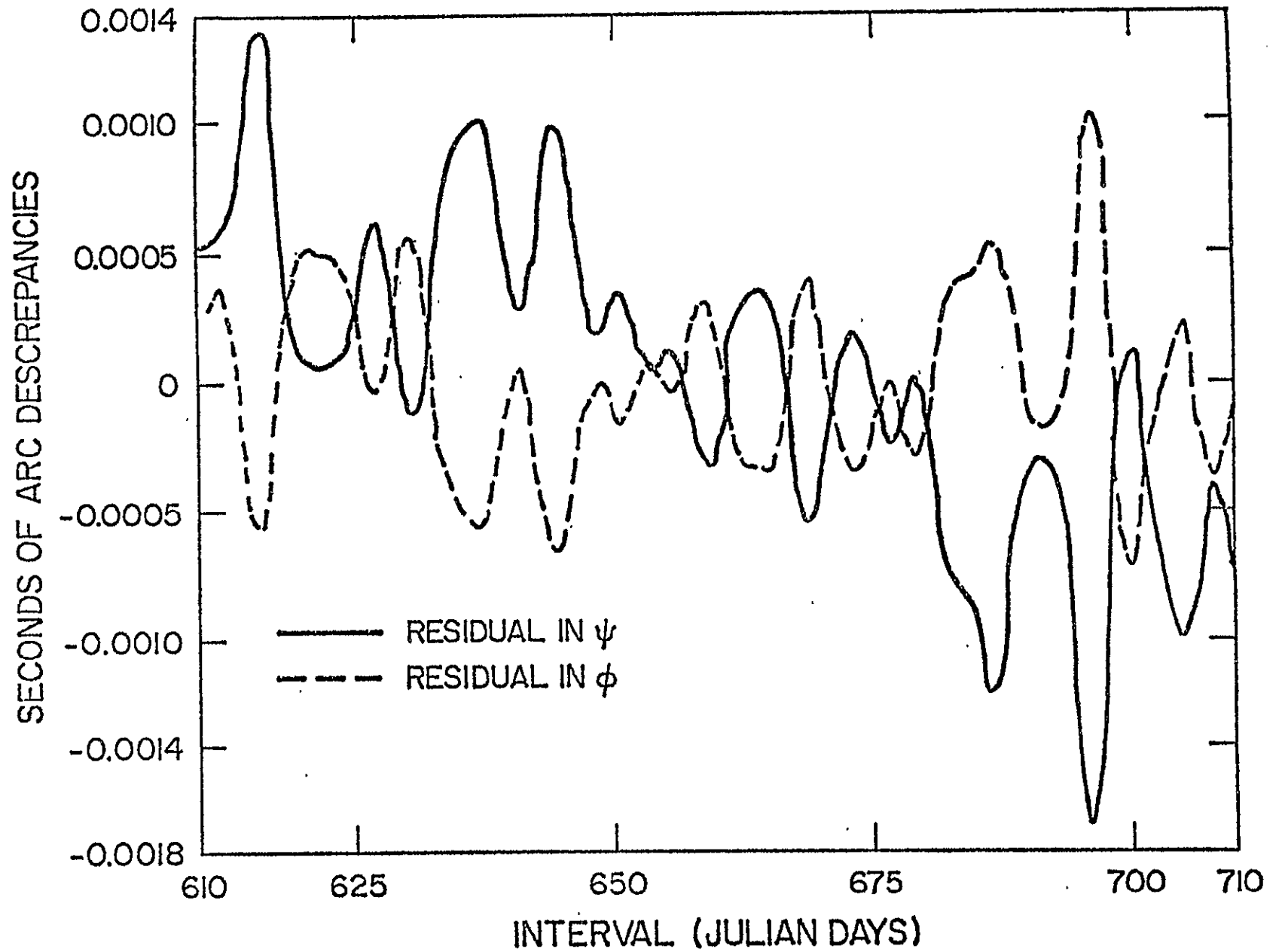
Fig. 2.1-4 Correlation between the Eulerian angles.

$$\phi = \int_{t_0}^{t} \dot{\phi} \, dt = k(t - t_0) - \int_{t_0}^{t} \dot{\psi} \cos \theta \, dt \qquad 2.1 - 22$$

so that

$$\frac{\partial \phi}{\partial k} = t - t_0 \qquad 2.1 - 23$$

With the above factors introduced in the numerical theory, an integration/adjustment was performed over a 100-day period with comparisons to classical theory as outlined in equation 2.1- 19 made at 0.25 day intervals. The sum squares of the residuals prior to adjustment was 0.3263 seconds squared and after adjustment 0.0001 seconds squared. The correlation matrix is given in Table 2.1-5 and a plot of the residuals in Fig. 2.1-5.

Table 2.1-5

Correlation Matrix for Numerically Integrated Eulerian

Angle Fit to Classical Theory

	θ	ψ	ϕ	$\dot{\theta}$	$\dot{\psi}$	k
θ	1.0	-0.055	0.034	0.074	0.41	0.004
ψ		1.0	-0.34	-0.74	-0.14	-0.013
ϕ			1.0	0.45	0.085	-0.76
$\dot{\theta}$				1.0	0.18	0.017
$\dot{\psi}$					1.0	0.009
k						1.0

24
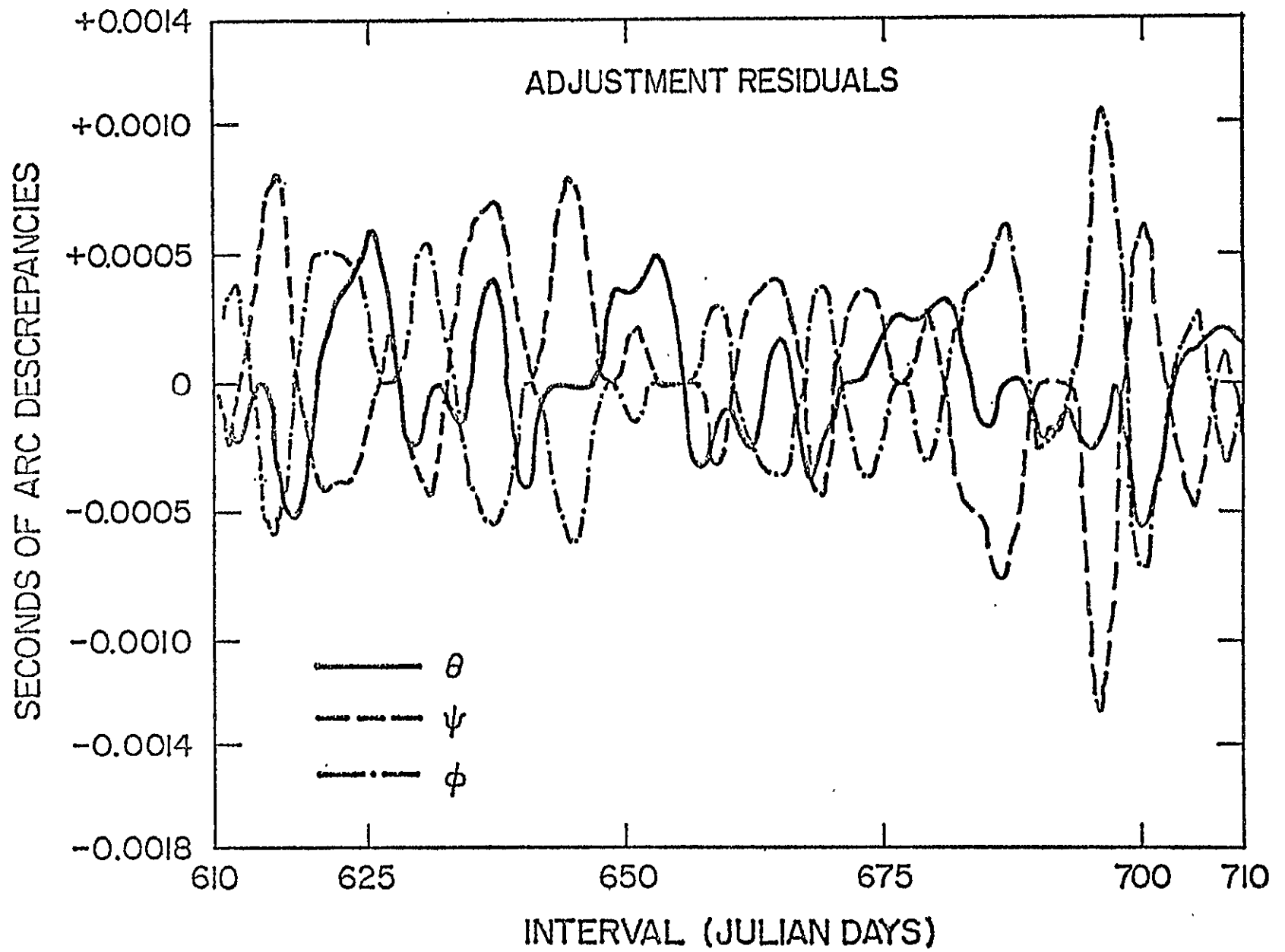
Fig. 2.1-5 Residuals of Eulerian angles.

2.2 Orientation of the Moon by Numerical Integration

H.B. Papo[1]

2.21 Introduction

The establishment of fundamental control on the moon is considered inseparable from the lunar ephemeris and the orientation of the moon in space. In the ideal case the control network, the lunar ephemeris and the orientation of the moon should form a consistent set of parameters and data. Analysis of the available lunar ephemerides led us to the adoption of JPL's DE-69 ephemeris as a basis of our system. For the orientation of the moon a new solution was developed as an integral part of a comprehensive data reduction system. As is well known, the model of physical librations of the moon together with Cassini's three laws provide the tool for defining the orientation of the moon in inertial space.

The problems associated with conventional analytical solutions for the physical librations of the moon which we addressed in our study are as follows:

(1) Difficulties introduced by the linearization of Euler's dynamical equations.

(2) Insuring an absolute consistency between the physical libration model and any ephemeris of the moon and the sun--in particular, a numerical ephemeris like JPL's DE-69.

(3) The need to identify and select a set of parameters which can be

---

[1]Presently at the Technion, Israel.

determined in a least squares analysis of given observational material.

Our present solution has succeeded in providing a satisfactory answer
to the foregoing problems. However, we have made no provisions as yet to
account for the partially elastic behavior of the moon.

2.22 General Principles

As a model for developing our approach, we considered procedures
analogous to orbit determination by numerical integration. The simplest
definition of such a model is as follows:

> The physical libration angles and their time rates (a total
> of six quantities) at an arbitrary epoch are assumed to be known.
> Using those as initial values, the physical libration angles at
> another epoch are obtained by numerically integrating the equations
> of rotational motion of the moon.

Thus, a solution for the physical librations of the moon by numerical
integration comprises the following:

(1) Derivation of differential equations of rotational motion of the
moon.

(2) Development of computational procedures for the solution of a set of
initial values of the physical libration angles and their time rates
at some epoch, as well as the solution of a number of physical
constants which govern the equations of rotational motion of the moon.

The coordinate systems involved in our analysis are the following
(Fig. 2.2-1): The origins of both XYZ and xyz Cartesian coordinate systems
is set at the center of mass of the moon. The XYZ system is parallel to
the mean ecliptic system: the X axis points to the mean vernal equinox of
date while the Z axis is normal to the plane of the ecliptic. The xyz
system, to be referred to as the selenodetic system, is fixed with respect

28
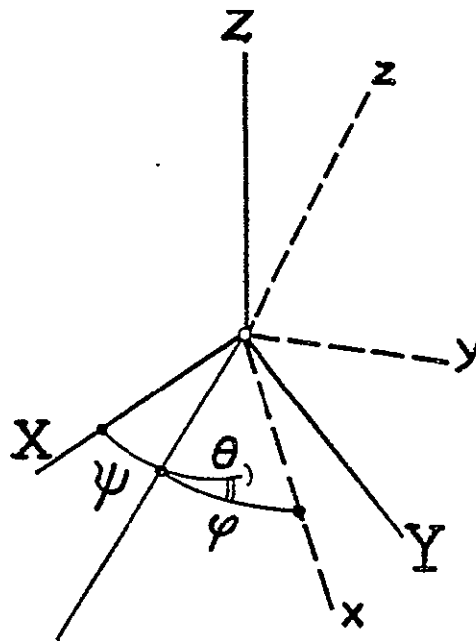
Fig. 2.2-1 Coordinate systems.

to the body of the moon and its axes x,y,z coincide with the principal axes
of inertia of the moon. The transformation between the two systems is
carried out through the three Eulerian angles ϕ, ψ, θ. The physical
libration angles τ, σ, ρ, are related to the three Eulerian angles ϕ, ψ, θ
(equation 2.2 - 1) through the respective mean longitude of the moon (L),
the longitude of ascending node of its mean orbit (Ω) and through the
mean inclination of the lunar equator with respect to the ecliptic (I):

$$\left| \begin{array}{c} \tau \\ \sigma \\ \rho \end{array} \right| = \left| \begin{array}{c} \phi + \psi \\ \psi \\ \theta \end{array} \right| - \left| \begin{array}{c} L - \pi \\ \Omega \\ I \end{array} \right| \qquad 2.2 - 1$$

2.23 Equations of Rotational Motion of the Moon

The rotational motion of the moon, regarded as a rigid body, around
its center of mass and with respect to an inertial frame of reference is
described by Euler's dynamical equations:

29

$$\begin{vmatrix} \dot{\omega}_x \\ \dot{\omega}_y \\ \dot{\omega}_z \end{vmatrix} = \begin{vmatrix} \alpha & 0 & 0 \\ 0 & -\beta & 0 \\ 0 & 0 & \gamma \end{vmatrix} \cdot \left\{ \frac{3\ k^2E}{r_E^5} \begin{vmatrix} yz \\ xz \\ xy \end{vmatrix}_E + \frac{3\ k^2S}{r_S^5} \begin{vmatrix} yz \\ xz \\ xy \end{vmatrix}_S - \begin{vmatrix} \omega_y & \omega_z \\ \omega_x & \omega_z \\ \omega_x & \omega_y \end{vmatrix} \right\} \qquad 2.2 - 2$$

The rotational velocity components of the moon around the x,y,z axes are denoted as ω_x, ω_y, ω_z, while $\dot{\omega}_x$, $\dot{\omega}_y$, $\dot{\omega}_z$ are the respective time rates of those velocities.

The coefficients α, β, γ are ratios between the principal moments of inertia of the moon as follows:

$$\alpha = \frac{C - B}{A}$$

$$\beta = \frac{C - A}{B}$$

$$\gamma = \frac{B - A}{C}$$

where A, B, C are the moments of inertia about x, y, z respectively.

The gravitational constants of the earth and of the sun are given as k^2E and k^2S respectively.

The selenodetic coordinates of the centers of mass of the earth and of the sun are given as $[x\ y\ z]_E$ and $[x\ y\ z]_S$ while r_E and r_S are the respective distances moon-earth (r_E) and moon-sun (r_S).

The relationship between the rotational velocities ω_x, ω_y, ω_z and the Eulerian angles and their time rates ϕ, ψ, θ, $\dot{\phi}$, $\dot{\psi}$, $\dot{\theta}$ is given by Euler's geometric equations:

$$\begin{vmatrix} \omega_x \\ \omega_y \\ \omega_z \end{vmatrix} = R_3(\phi)\ R_1(-\theta) \left\{ \begin{vmatrix} -\dot{\theta} \\ 0 \\ \dot{\psi} \end{vmatrix} + R_3(\psi) \begin{vmatrix} e_x \\ e_y \\ e_z \end{vmatrix} \right\} + \begin{vmatrix} 0 \\ 0 \\ \dot{\phi} \end{vmatrix} \qquad 2.2 - 3$$

30

The symbols $R_3(\phi)$, $R_1(-\theta)$, etc. represent orthogonal rotation matrices in the conventional sense.

The only new feature in these equations is the vector $[e_x, e_y, e_z]$ which represents the small rotational velocity of the X,Y,Z system with respect to an inertial frame of reference. This motion results from the motion of the ecliptic and the regression of the vernal equinox. We should note that e_x and e_y are relatively small quantities.

We differentiate Euler's geometric equations with respect to time and substitute the results in Euler's dynamical equations. After some regrouping, the results are the second-order differential equations of the Eulerian angles of the moon:

$$
\begin{vmatrix} \ddot{\phi} \\ \ddot{\psi} \\ \ddot{\theta} \end{vmatrix} = W^{-1} \left\{ \begin{vmatrix} \alpha & 0 & 0 \\ 0 & -\beta & 0 \\ 0 & 0 & \gamma \end{vmatrix} \left(\frac{3k^2 E}{r_E^5} \begin{vmatrix} yz \\ xz \\ xy \end{vmatrix}_E + \frac{3k^2 S}{r_S^5} \begin{vmatrix} yz \\ xz \\ xy \end{vmatrix}_S - \begin{vmatrix} \omega_y & \omega_z \\ \omega_x & \omega_z \\ \omega_x & \omega_y \end{vmatrix} \right) \right.
$$

$$
- \left[\frac{\partial R_3(\phi)}{\partial \phi} \cdot R_1(-\theta)\dot{\phi} + R_3(\phi)\,\frac{\partial R_1(-\theta)}{\partial \theta}\,\dot{\theta} \right] \left\{ \begin{vmatrix} -\dot{\theta} \\ 0 \\ \dot{\psi} \end{vmatrix} + R_3(\psi) \begin{vmatrix} e_x \\ e_y \\ e_z \end{vmatrix} \right\}
$$

$$
\left. - R_3(\phi)\,R_1(-\theta)\,\frac{\partial R_3(\psi)}{\partial \psi}\,\dot{\psi} \begin{vmatrix} e_x \\ e_y \\ e_z \end{vmatrix} \right\} \qquad\qquad 2.2 - 4
$$

All the symbols in these equations have been explained already except for W^{-1} which is a 3 x 3 matrix composed of functions of θ and ϕ.

In principle, these three equations can be used for numerical integration of the Eulerian angles. However, due to the large numerical values of ϕ, ψ, θ and also due to a strong negative correlation between ϕ and ψ,

31

it is advantageous to perform another transformation and obtain differential equations of the physical librations. This is similar to a transformation from Cowell's to Encke's equations of motion of a satellite.

By repeated differentiation of equations 2.2 - 1, we arrive at the final result to be referred to as the differential equations of rotational motion:

$$\begin{vmatrix} \ddot{\tau} \\ \ddot{\sigma} \\ \ddot{\rho} \end{vmatrix} = \begin{vmatrix} \ddot{\phi} + \ddot{\psi} \\ \ddot{\psi} \\ \ddot{\theta} \end{vmatrix} - \begin{vmatrix} \ddot{L} \\ \ddot{\Omega} \\ 0 \end{vmatrix} \qquad\qquad 2.2 - 5$$

where $\ddot{L}$ and $\ddot{\Omega}$ are composed of power series of time with fixed coefficients.

2.24 Least Squares Analysis

The numerical solution of the differential equations of rotational motion of the moon (2.2 - 5) depends on two sets of parameters which are subject to estimation, namely:

(1) The values of the physical libration angles and their time rates at an arbitrary epoch. Those values will be referred to as the initial values (ξ_0).

(2) A number of constants which appear on the right-hand side of the differential equations.

We should note at this point that the ephemeris data and also the gravitational constants of the earth and the sun which are associated with the ephemeris are treated in our analysis as being fixed. The same applies to the vector $[e_x, e_y, e_z]$.

The only parameters which are subject to change and which are being estimated in the least squares sense are the ratios α, β, γ. As the three

32

are interrelated by a well-known identity, we consider only two quantities to be referred to as the physical constants (λ). Those could be α and β or the traditional f and γ where

$$f = \frac{\alpha}{\beta}$$

The above parameters can be estimated from the analysis of any type of observational material which is, in general, sensitive to the orientation of the moon. Heliometer observations, photography by long focus astronomical telescopes or laser ranging to retroreflectors placed on the moon surface could be used for this purpose.

Each type of observation is associated with a typical set of additional parameters which pertain to the instrumentation and to the particular observational mode being used. This last group of parameters will be referred to as observation constants (μ).

Each observation can be modeled by the generally nonlinear model F:

$$F = F(\xi_0^a, \lambda^a, \mu^a) \qquad \qquad 2.2 - 6$$

According to the standard procedure in least squares estimation, we proceed by linearization of the model F in terms of the parameters and obtain the observation equations:

$$V = \frac{\partial F}{\partial \xi_0^a} \xi_0 + \frac{\partial F}{\partial \lambda^a} \lambda + \frac{\partial F}{\partial \mu^a} \mu + F(\xi^o, \lambda^o, \mu^o) - F^b \qquad 2.2 - 7$$

We will pay closer attention to the coefficients of ξ_0 and λ. The partial derivative $\partial F / \partial \mu$ does not present any particular problem, and it is irrelevant to the numerical integration process. The two coefficients $\partial F / \partial \xi_0$ and $\partial F / \partial \lambda$ can be broken into the following forms:

$$\frac{\partial F}{\partial \xi_0^a} = \frac{\partial F}{\partial \xi} \cdot \frac{\partial \xi}{\partial \xi_0^a} = A_\xi U$$

$$\frac{\partial F}{\partial \lambda^a} = \frac{\partial F}{\partial \xi} \cdot \frac{\partial \xi}{\partial \lambda^a} = A_\xi Q$$

$\partial F/\partial \xi$ are the partial derivatives of the observational model F with respect to ξ--the current values of the physical libration angles and their time rates. These partial derivatives ($\partial F/\partial \xi$), like the ones above ($\partial F/\partial \mu$), are irrelevant to the numerical integration procedure.

The two matrices U and Q represent the partial derivatives of the current physical libration angles and time rates (ξ) with respect to the initial values (ξ_0) and again with respect to the physical constants (λ), respectively. In the literature on orbit determination these two matrices are referred to as the state transition (U) and the parameter sensitivity (Q) matrices. We should notice the important fact that U and Q are independent of the particular type of observation being used.

2.25 Comparison to an Analytical Solution

To test our solution we chose as a standard Eckhardt's 1970 model for the physical librations as published in [Eckhardt, 1970, p. 267]. After an extensive analysis we selected the function to be minimized by the least squares procedure as the sum of squares of $\Delta \tau$, $\Delta \sigma$ sinθ and $\Delta \rho$. Here the Δ's represent the differences between the numerically integrated and Eckhardt's values at each epoch of comparison.

We ran an adjustment over about 1400 days, taking Eckhardt's angles at intervals of three days. The residuals after the adjustment, reduced to an amplitude of 2 to 3 seconds of arc, except for the residuals in τ which displayed a clearly periodic character with large amplitude and a period of roughly three years. The adjusted values for β and γ agreed

with Eckhardt's values as given in the paper mentioned above.

We changed the initial epoch by several hundred days, adjusted again, and found that the residuals persisted with only minor differences. This demonstrated the stability of our solution (see Fig. 2.2-2).
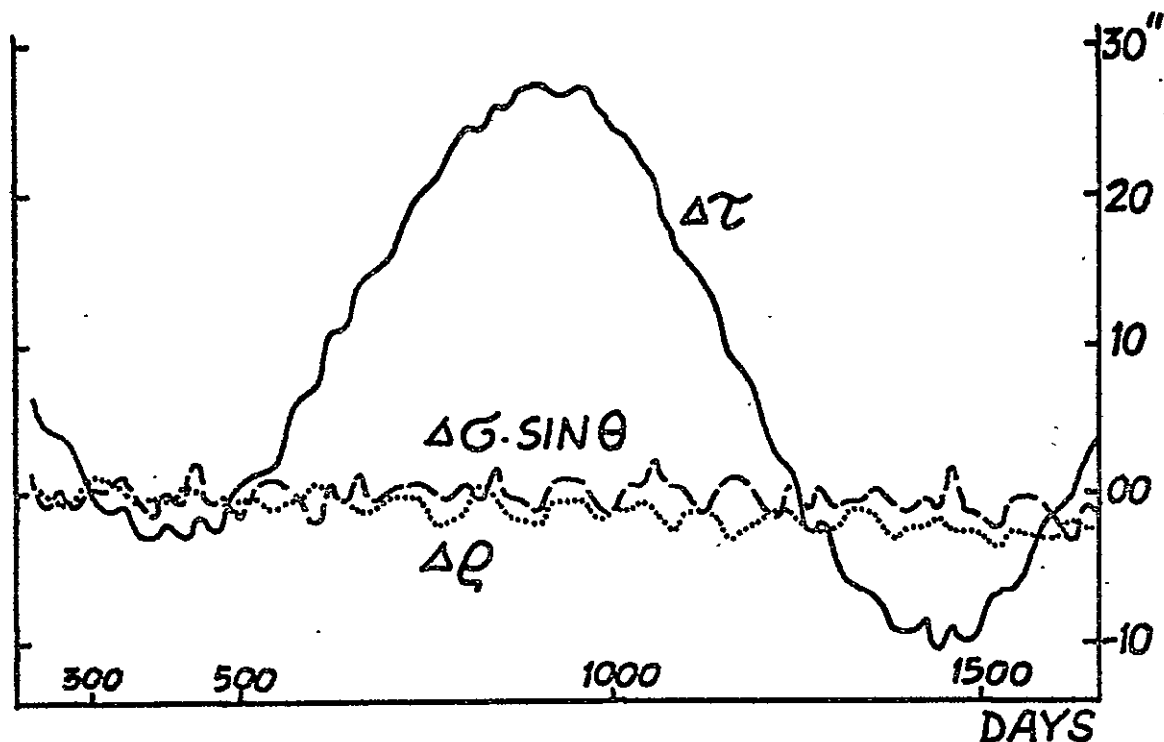
Fig. 2.2-2 Comparison to Eckhardt (1970).

It was thought that the large differences in τ were due to some inconsistency. The integrated physical libration angles were obtained through the use of the JPL DE-69 ephemeris, while Eckhardt used Brown's ephemeris without the additive and the planetary terms in the lunar theory [Eckhardt, 1967, p. 51]. Eckhardt's angles augmented by the inclusion of the effect of the additive and planetary terms [Williams, 1973] were used again as a new standard.

The new adjustment over the same interval as above resulted in a significantly improved fit. The residuals in $\Delta\tau$ and in $\Delta\rho$ dropped below

35

the 1" level while in Δσ sinθ there was still a one monthly term with an amplitude of 2"5 (see Fig. 2.2-3). The same period was indicated by the much smaller residuals in Δρ.
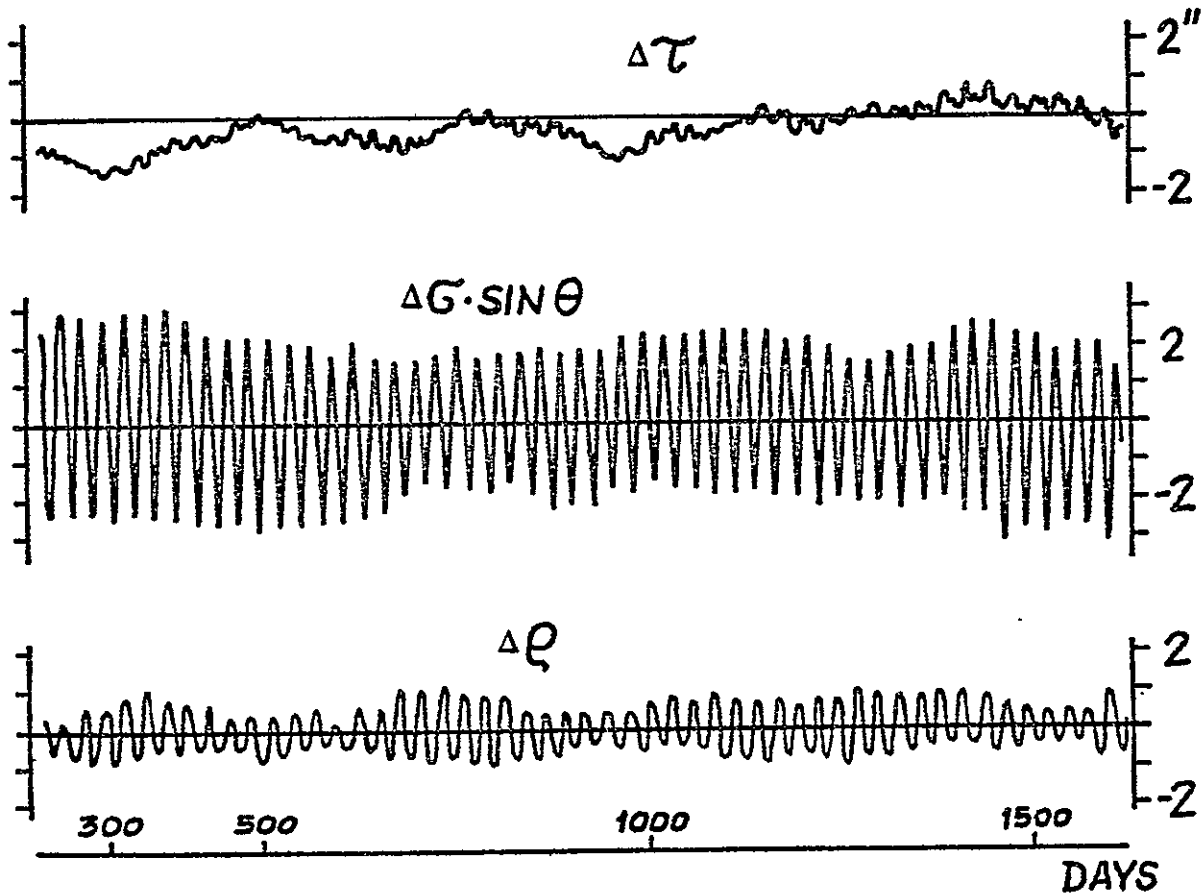
Fig. 2.2-3 Comparison to Eckhardt augmented for additive and planetary terms.

We concluded our experiments of fitting to an analytical solution, having shown that the two methods are fairly compatible over an extended period of time. The next test of our method would be made through the analysis of real data which is sensitive to the physical librations of the moon.

36

2.3 Simulated Earth-Moon Environment

H.B. Papo[1]

2.31 Introduction

As in any simulation, the primary goal is to generate absolute data which will be entirely self-consistent and, in addition, will resemble as closely as possible the true environment.

After exploring briefly several possibilities the way chosen was to use numerical integration of the equations of motion (translation as well as rotation) of the earth, the moon, and a satellite orbiting the moon.

The following sets of data are generated:

(a) Geocentric ephemeris of the moon in a fixed celestial coordinate system.

(b) Eulerian angles for orienting an earth-fixed coordinate system vs. the same inertial celestial system mentioned in (a).

(c) Eulerian angles for orienting a moon-fixed coordinate system to the inertial celestial system.

(d) Selenocentric ephemeris of a moon-satellite in the inertial celestial system.

(e) Range and range-rate from four tracking stations on earth to the satellite of the moon.

_____

[1]Presently at the Technion, Haifa, Israel.

(f) Optical bundles of rays from three observatories on earth or from a

satellite orbiting the moon. Each ray represents the unit vector of

the line connecting the projection center to a given triangulation

point on the moon in a specially oriented reference frame. The case

is demonstrated in the diagram below.

PC   - projection center

B_1,B_2,B_3 - reference frame oriented vs.
            the inertial coordinate system
            through three Eulerian angles

TP   - triangulation point on the
            moon, M

B_1 axis - points to the moon's center

B_2 axis - is parallel to the XY plane of
            the inertial system

B_3 axis - completes a right-handed
            Cartesian system
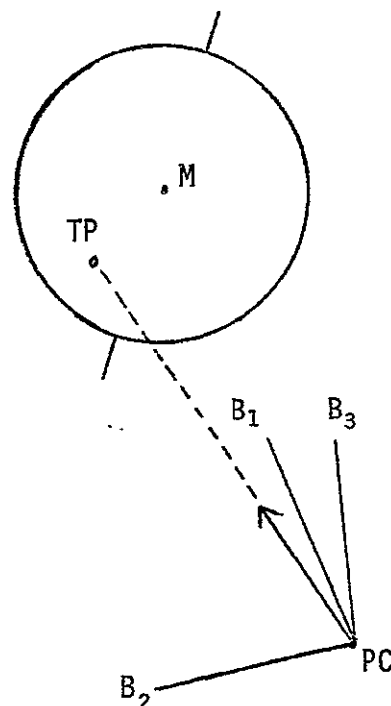
2.32 Qualitative Description of the Simulation

The only celestial bodies considered in the system are the earth and

the moon. The fixed (inertial) celestial coordinate system is chosen

parallel to the mean ecliptic system of a given standard epoch. However,

no stars are provided to serve as reference for inertial space.

2.321 The Earth.

The earth is a perfectly rigid body having a topography identical to

the true earth. A Cartesian coordinate system centered at the earth mass

center and coinciding with the principal axes of inertia is defined fixed

to the earth body and following identically the UVW--average terrestrial

system of the true earth: W passing through the CIO pole, plane UW

containing Greenwich. The equatorial semi-axis and the flattening of the reference ellipsoid are the same as the ones adopted by IAU in 1964.

Four radio tracking stations (range and range-rate) and three optical observatories are defined at locations where actual and presently active stations are engaged in observations of the appropriate type.

Dynamically the earth is rotationally symmetric. The spherical harmonics expansion of the earth gravity field has only one coefficient-- J_2--different from zero. The mass of the earth and the value of J_2 are identical with the values adopted by the IAU in 1964. Choosing a value for the ratio between the polar and the equatorial moment of inertia $(C - A)/C$ was a rather complicated matter. The value adopted finally was the one consistent with the nutation constant in obliquity $N = 9.''21$. The value calculated by using Sir H. Jeffrey's formulae differs slightly from the one adopted.

The orientation of the UVW system was taken from the American Ephemeris and Nautical Almanac series for the sun. Its rate of diurnal rotation was determined in accordance with Newcomb's equation. These served as the initial values in the integration.

2.322 The Moon.

The moon is a perfectly rigid body. Its topography is that of a sphere with radius equal to the mean radius of the true moon. Its center of mass is shifted with respect to the center of the sphere towards the earth. On the "front" side of the moon (facing the earth) 30 triangulation points are chosen evenly spaced and in areas on the true moon where there is an abundance of craterlets of the 3-7 km diameter range. The crater Mösting A

and also the crater Bruce in Sinus Medii are among the 30 points. A Cartesian coordinate system fixed to the body of the moon, centered at its mass center and following the orientation of the selenographic coordinate system (x,y,z) is defined. The xyz axes are identical with the principal axes of inertia.

The mass of the moon is related to that of the earth by the ratio 1/m identical to the one adopted by IAU in 1964.

Dynamically the moon is a more complicated body than the earth. It is a triaxial ellipsoid with a set of 12 point masses superimposed on its triaxial dynamic shape. In terms of coefficients of spherical harmonics expansion $C_{2,0}$ and $C_{2,2}$ are the only nonzero second-order coefficients. Their values were taken identical to the ones used by NASA. The mascons are selected in general at locations corresponding to actual mascons as published recently. There are several additional mascons introduced, some of them negative, selected to satisfy certain conditions. The conditions that the total of 12 mascons satisfy are that their total mass and also their first and second moments are all zero. This was found necessary in order to retain a basically rough gravity field as far as a close moon satellite is concerned and at the same time not to complicate unnecessarily the equations of motion of the moon vs. the earth.

The three moments of inertia (A,B,C) are consistent with the $C_{2,0}$ $C_{2,2}$ values and correspond to a ratio $\beta = (C - A)/B$ identical to the presently accepted value of β.

The initial orientation and rates of rotation of the moon's xyz system are taken from Eckhardt's model.

2.323 Lunar Satellites.

A spacecraft of negligible mass is defined in which no parallax exists between its mass center, the calibrated point of the transponder for radio measurements and the principal point of its camera. No orientation jets or other physical effects disturb its perfectly gravitational motion. In designing the various satellite orbits no consideration is given to their trajectories prior to the circumlunar orbit.

2.324 Illuminating Source "Sun".

An illuminating nongravitational "sun" is defined rotating on the XY fixed celestial plane at an infinite distance from the earth-moon system. Its angular rotation speed corresponds to that of the mean sun as given by Newcomb's equation.

2.325 General Notes.

(a) In generating the optical, range and range-rate data all the practical considerations of visibility, illumination of target, photography away from the sun, minimum altitude angles for earth photos, maximum field angle of camera, etc. are enforced. If any of the conditions outlined necessary for the existence of an observation is violated, the tentative observation is replaced by zero.

(b) The computer programs developed to generate the simulated environment are based on Encke-type integration, i.e., only the perturbations to the reference cases are integrated, thus increasing the number of significant figures in the quantities needed in the simulation.

2.33 Constants Used in the Simulation

Earth

K^2E = .297556 × 10^{16} km^3/day^2 - gravitational constant

J_2 = .0010827 - second zonal harmonic

a = 6378.16 km - equatorial semi-diameter

f = 1/298.25 - flattening of reference ellipsoid

$\frac{C - A}{C}$ = .00327802 - A, C--equatorial and polar moments of inertia

ω_3 = 6.300388098 rad/day - diurnal rotational speed

No.	Name	Type	U	V	W
1	Tucson	OPT	-1996.0051	-5042.6961	3360.7748
2	Pic du Midi	OPT	4686.1252	11.6385	4331.0499
3	Johannesburg	OPT	5058.2628	2698.0251	-2799.8019
4	Goldstone	RRT	-2351.1949	-4655.5944	3661.0605
5	Woomera	RRT	-3978.5840	3724.8986	-3302.3278
6	Johannesburg	RRT	5085.4787	2668.3035	-2768.7011
7	Madrid	RRT	4845.7274	- 360.0147	4125.7615

Moon

m = 81.3 - ratio of mass of the earth to that of the moon

$C_{2,0}$ = -.000207
$C_{2,2}$ = .0000207 - second-order harmonics

α = 3.6696 - ratio of equatorial semi-axis of earth ellipsoid to mean radius of the moon

β = .000629 - β = (C - A)/B ratio between moon's principal moments of inertia

Mascons in 10^{-6} Units of the Total Mass of the Moon

Situated on the Surface of the Moon Sphere

No.	Mass	Selenographic	
		Longitude	Latitude
1	+19.0694	-15°	15°
2	-20.0394	20	20
3	15.3805	30	- 5
4	-11.8910	0	-20
5	11.7378	-45	-40
6	-12.7844	-50	- 5
7	2.8233	-60	30
8	- 6.0431	-15	60
9	10.0246	50	50
10	- 8.0542	70	10
11	8.1149	60	-30
12	- 8.3384	30	-60

Triangulation Points on the Surface of the Moon Sphere

No.	λ	φ	No.	λ	φ
1	-30°	79°	16	50°	7°
2	70	63	17	- 5	- 3
3	-74	51	18	-73	-14
4	-27	52	19	26	-16
5	18	57	20	80	-10
6	77	40	21	-42	-20
7	-47	31	22	- 5	-29
8	- 3	33	23	51	-23
9	38	38	24	-78	-44
10	-78	18	25	-28	-41
11	-27	13	26	35	-42
12	19	16	27	68	-46
13	78	18	28	5	-57
14	-48	4	29	-45	-72
15	0	1	30	50	-74

Illuminating "Sun"

ϕ_0 = 1.7399359 rad

ϕ_1 = .0172027913 rad/day

constants in the equation giving the longitude of the illuminating vector

$$\phi = \phi_0 + \phi_1 (T - T_0)$$

T_0 - standard epoch

1900.0 ≡ 2415020.0 J.D.

T - epoch in J.D.

3. POSITION DETERMINATION FROM EARTH-MOON OBSERVATIONS

3.1 Lunar Far Side Positions from Apollo Trans-Earth Trajectory Photography

M.D. Sprague[1] and W. Riotte[2]

3.11 Summary of Theoretical Approach

The investigation into the feasibility of extending selenodetic control on the far side of the lunar surface through an analytical photogrammetric method utilizing simulated Apollo trans-earth trajectory photography was completed [Sprague, 1971].

A brief summary of the theoretical approach to the problem, major conclusions and recommendations are presented here. The theoretical procedure of the work was to generate synthetic photographic data of thirty triangulation points on the lunar surface far side as if taken with an 80 mm Hasselblad hand-held camera from the Apollo command module during the initial phase of the vehicle's trans-earth trajectory. Such simulated "photos" were generated mathematically at one minute intervals over a forty-minute period (from TEI + 20 minutes to TEI + 1 hour) for four separate simulated Apollo missions. The data was generated from the simulated earth-moon environment program developed in [Papo, 1971]. This

---

[1]Presently with the U.S. Army

[2]Presently with the U.S. Air Force

generated photo data, in the form of photo coordinates of triangulation points and photo exterior orientation, plus survey coordinates of the triangulation points, was randomly perturbed within specified limits to simulate observational errors and then subjected to a block triangulation adjustment calculation. Thus, adjusted values of triangulation point survey coordinates, photo coordinates and exterior orientation are obtained. Triangulation points in the lunar equatorial band were used as known control points and their coordinates were constrained to ±300 meters in the adjustment. After adjustment, the adjusted values of the lunar survey coordinates for the triangulation points appearing on photos used in the adjustment were compared with the corresponding true or theoretical coordinate to determine the degree of success of the method.

The block triangulation performed with theoretical data in this investigation differs from a conventional (earthbound) block triangulation in two major respects. First, a conventional block normally has control points established around the perimeter of the block with some additional control within the block's interior. In this study, control points are established in a band or strip and appear through the center or along the edge of the block of photos depending upon the spacecraft trajectory. The second major difference lies in the pattern of photos in the block and the photo overlap resulting. For conventional blocks, the flight path and exposure timing is such that 60 percent end overlap and 30 to 60 percent side overlap is used for all photos within the block. Also, the photography is flown at approximately the same altitude above the terrain so that each photograph covers an area of nearly equal size. In the case of the lunar post-TEI photography, each successive photo is exposed with the

exposure station at a greater distance from the surface than for the preceding photograph. Therefore, each photo contains a larger area of the surface than the one taken before it. A point is quickly reached in the post-TEI trajectory when photo overlap is 100 percent (for one-minute photo interval), i.e., all points in the preceding photo are contained in the next photo exposed.

3.12 Results of Simulated Block Triangulation Adjustments

In the course of the investigation, block triangulation adjustment calculations were done with various sets of simulated photo data. The purpose was to experiment with numbers of photos used, camera "look angles" and time interval between "photos" used. Initially, various six-photo block adjustments were done for each of the four individual simulated trajectories. Then block adjustments were performed with increasing numbers of photo data sets up to a maximum of 16 photos both for single trajectories and for combinations of "photos" from two, three and four trajectories.

Results of the triangulation adjustments in all cases indicated that some improvement was obtained in the adjusted location of a triangulation point compared to the initial perturbed or "unknown" location of that point. The degree of improvement was seen to be directly related to the number of photographic observations (number of photos the point appeared on), the number of trajectories or missions from which the point may be photographed, and the geometrical relationship between the point and the exposure stations.

The study revealed that the area of lunar surface on the far side for which this procedure may be effectively applied is severely restricted due to the very nature of the spacecraft trajectory after TEI. In order for the

vehicle to be placed in the proper trajectory to return to earth, the TEI burn must occur on the lunar far side near the 180° meridian, and by 20 minutes after the injection burn, the spacecraft has proceeded in its trajectory to a point some 1200 to 1400 km from the surface and in the vicinity of the 100° to 120° E meridian. This, then, precludes the opportunity to photograph areas further east than approximately 130° to 135° E on the surface. Also, the position of the terminator may eliminate a large portion of area for photography depending upon the terminator location.

The standard deviations for selenographic (lunar survey) coordinates of new extended control (NEC) points obtained in the results provides a means of comparing final adjusted value to the true or theoretical value of a coordinate.

Inspection of the results of the block adjustments revealed certain similarities: (a) The path of the subvehicle point on the lunar sphere is the determining factor for the "observability" of a triangulation point (provided the point is illuminated). (b) A stronger solution (in terms of lower standard deviation and residuals) was obtained for those triangulation points nearest the subvehicle path and thereby appearing on a maximum number of photos included in the block adjustment. Points located at great distances from the track, such as the points at extreme northern latitudes and points east of the 120° E meridian, are not included in the photographic coverage until late in the period in which photography is taken. Thus, these points appear as fewer observations in the adjustment and the geometry of intersecting conjugate rays result in a weaker solution.

(c) It was noted throughout the study that standard deviations for Y-coordinates of triangulation points was larger than for either the X or

Z coordinate. It was concluded that the reason for this was due to the location of the exposure stations with respect to the triangulation points. Fig. 3.1-1 illustrates the geometry involved. Primarily due to the curvature of the lunar surface, observations on points at substantial distances away from the subvehicle point introduce larger errors in the direction of the Y-coordinates than in either the X or Z direction for any small angular error δ. For points near the subvehicle point, such as point A in Fig. 3.1-1 (a) and (b), a small angular error in the direction of the optical ray produces small errors δZ and δX in position as shown. However, for points at increasingly larger distances from the subvehicle point as point B, the error in δY becomes dominant and is much greater in size than δX or δZ for points near the subvehicle point. This analysis holds true for exposures taken with the optical rays from the surface to the projection center lying primarily in the Y-coordinate direction as was the case for all four of the simulated missions.

(d) In all cases as the number of photos in the block adjustment was increased, the values for standard deviations of survey coordinates decreased. Table 3.1-1 presents a comparison of the standard deviations for five representative NEC points resulting from four different block adjustments with simulated photo data from the Apollo 12 mission.

In general, for sixteen-photo adjustments of photo data from single simulated missions, standard deviations for X and Z selenographic coordinates of NEC points were under 1.0 km, while the standard deviations of Y-coordinates were under 1.5 km.

(e) Finally, results obtained through block adjustment of combined photo data taken from two or more simulated missions were much more promising

49 .
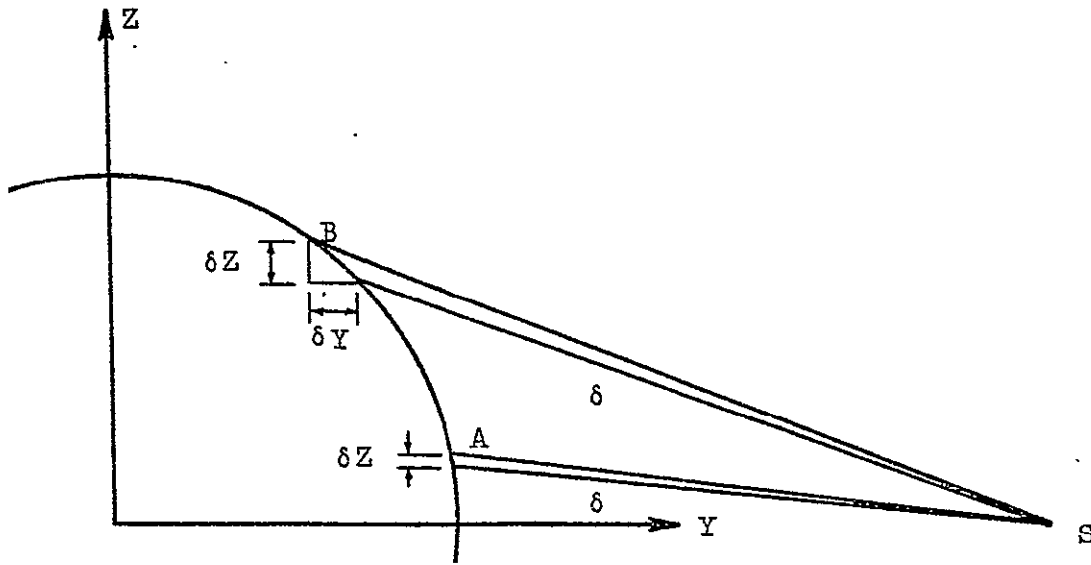
a) Y - Z Plane.
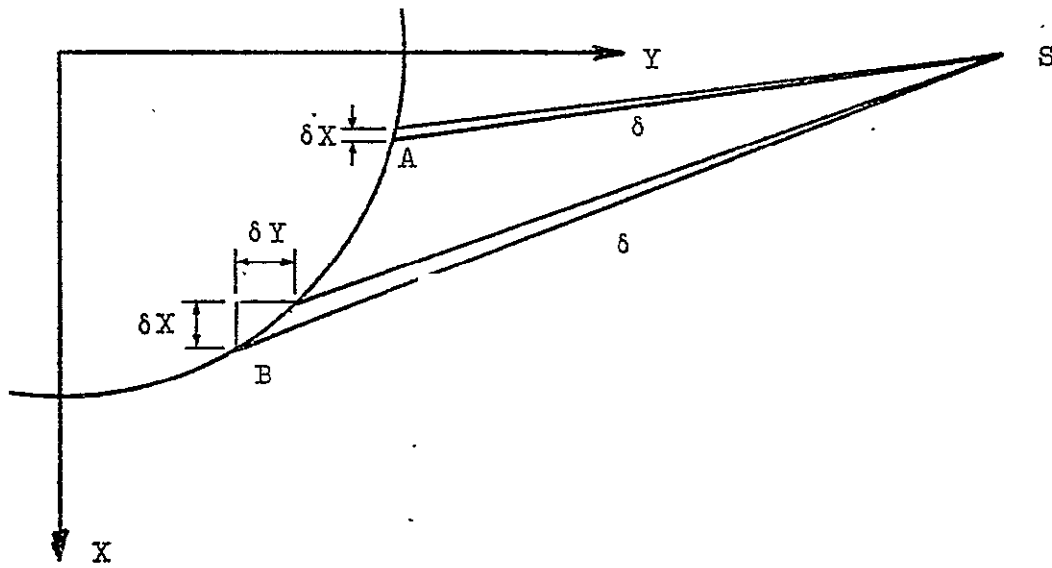
b) X - Y Plane.

Fig. 3.1-1   Errors in X,Y,Z selenographic coordinates.

50

Table 3.1-1

Comparison of Standard Deviation for Five Representative NEC Points
from Block Adjustments of the Simulated Apollo 14 Mission.

NEC Pt. #	Std. Dev.	6 Block Block (km)	10 Photo Block (km)	12 Photo Block (km)	16 Photo Block (km)
12	σx	0.550	0.536	0.497	0.248
	σy	1.121	1.088	0.977	0.563
	σz	0.218	0.202	0.184	0.132
		(6)	(10)	(12)	(16)
15	σx	1.427	1.042	0.925	0.844
	σy	2.335	1.790	1.549	1.384
	σz	0.617	0.497	0.425	0.378
		(5)	(9)	(11)	(13)
17	σx	0.232	0.154	0.157	0.122
	σy	1.132	0.865	0.750	0.482
	σz	0.330	0.264	0.232	0.173
		(5)	(9)	(11)	(14)
20	σx	1.608	0.326	0.317	0.192
	σy	4.041	1.139	0.992	0.603
	σz	1.253	0.441	0.378	0.261
		(3)	(7)	(9)	(12)
23	σx	3.169	0.957	0.833	0.762
	σy	6.613	2.522	2.017	1.738
	σz	2.209	0.978	0.761	0.644
		(2)	(5)	(7)	(9)

(Numeral in parenthesis is the number of photos on which the point
appears.)

than results secured through adjustment of single trajectory data. The
sixteen-photo block adjustments performed using photo data from all four
simulated missions achieved the strongest solution in that standard devia-
tions of coordinates were uniformly low for all NEC points appearing on
photos from at least two of the four missions as shown in Table 3.1-2.

Table 3.1-2

Standard Deviation of Selenographic Coordinates (in meters) for NEC Points Resulting from Sixteen-Photo Adjustments of Combined Mission Data

NEC Point No.		No. of Traj. Cont. Observ.	Job 1245 (TEI 25 to 49) 4 4min	Job 1246 (TEI 32 to 56) 4 4min	Job 1247 (TEI 22 to 60) 2 min	Job 1248 (TEI 30 to 60) 2 min	Max. Diff. (m)
12	σ_x	4	107m	134m	101m	137m	36
	σ_y		219	237	207	241	34
	σ_z		101	113	98	113	15
13	σ_x	4	94	107	88	108	20
	σ_y		213	212	212	216	40
	σ_z		92	102	86	101	16
15	σ_x	2	696	612	691	669	84
	σ_y		953	799	941	908	154
	σ_z		303	252	295	277	51
16	σ_x	4	99	121	102	122	23
	σ_y		168	226	168	228	60
	σ_z		96	108	102	108	12
17	σ_x	4	122	110	120	109	13
	σ_y		272	241	273	246	32
	σ_z		124	109	121	109	15
19	σ_x	3	163	203	267	243	104
	σ_y		344	394	470	418	126
	σ_z		185	183	226	196	43
20	σ_x	4	112	121	128	137	25
	σ_y		213	257	247	277	64
	σ_z		113	117	127	126	14
23	σ_x	4	138	152	161	199	61
	σ_y		306	324	342	393	87
	σ_z		130	133	148	157	27
24	σ_x	4	147	156	156	177	30
	σ_y		339	362	349	406	67
	σ_z		142	141	151	159	18
28	σ_x	1	251	726	328	1603	1352
	σ_y		1761	5176	2010	8133	6372
	σ_z		408	977	471	1465	1048
29	σ_x	2	194	227	217	279	85
	σ_y		698	630	725	678	95
	σ_z		219	209	239	241	32
30	σ_x	1	302	475	406	1229	927
	σ_y		1636	4854	1846	7995	6359
	σ_z		385	909	441	1417	1032

This theoretical investigation has provided substantiation for the premise that the photogrammetric method of block triangulation through least-squares adjustment of post-TEI photos of the moon can provide a means of significantly improving selenodetic control on the lunar surface.

The basic assumptions used throughout the procedure are listed below and they may also serve as limiting criteria for processing real data in preparation for block adjustment of actual mission photographs.

(1) Standard deviation of photo coordinates (1σ value) is 10 micrometers.

(2) Standard deviations for coordinates of those triangulation points used as control within the block are 300 m or less.

(3) Initial approximations for coordinates of NEC triangulation points under investigation are available with an accuracy of ±10 km.

(4) Initial approximations for the elements of exterior orientation may be determined (by single-photo resection) to within 100 km for the exposure station coordinates and to within ±10° for the angular elements.

With the above presuppositions in force, it is expected that improved selenographic coordinates for triangulation points may be obtained with resultant standard deviations of the order of 300 m to 1000 m if photo data from four or more Apollo missions with widely separated trajectories are subjected to the block triangulation adjustment.

The conditions under which the optimum solution was achieved using simulated data were:

(1) Photo data was extracted for use from four different simulated trajectories or missions which had widely separated subvehicle tracks.

53

(2) Four "photos" were selected from each of the four missions at four-minute intervals to comprise a sixteen-photo block.

(3) Photos used were spread uniformly over a time period of thirty minutes from TEI + 20 minutes to TEI + 50 minutes.

It is felt that the application of this method to post-TEI photography of the Apollo missions used in conjunction with the data reduction of other observational systems can contribute substantially in improving the existing selenodetic control net.

3.13 Results from Apollo 15 Trans-Earth Photography

The investigation towards the improvement of selenodetic control on the lunar limb through an analytical photogrammetric method utilizing Apollo 15 trans-earth photography was also completed [Riotte, 1972]. A brief summary of the problem, procedure, conclusions and recommendations are presented here.

It was shown earlier that it is theoretically feasible to extend control from points of known location to unknown points on the lunar surface through the use of photogrammetric techniques with Apollo metric photography taken after the spacecraft leaves the moon's orbit. This project answers the question "Can this be accomplished with real data?"

The successful Apollo 15 mission launched on July 26, 1971 was the first to carry a complete set of mapping cameras. The SIM (Scientific Instrument Module) contained among other items the Fairchild 3-inch mapping camera, a 3-inch stellar camera, and the ITEK 24-inch optical panoramic camera. This report used only the film from the 3-inch mapping camera.

The metric camera's 4-1/2" x 4-1/2" format contained an array of 121 reseaus and the calibrated coordinates of the reseaus were available from the calibration report.

During the lunar orbits the metric camera took continuous pictures of the lighted portion of the lunar surface and continued taking pictures after the TEI (Trans-Earth Injection). It is this series of pictures with the moon receding from view that was used in this project. A formated picture is shown as an example in Fig. 3.1-2. There are several factors that should be noted from an evaluation of this sequence of pictures: (a) The trajectory during TEI is well below the equator; (b) there is a narrow band (approximately 20° longitude, 85°-105° E) of visible features bordered on one side by the highly reflective surface and on the other by the terminator; (c) the base height ratio between pairs of photographs is extremely small (approximately 0.04) and well below the desired limit of 0.3 thus giving rear vertical photographs; (d) all measured photographs show 100% overlap; (e) the control points are found only on the photographed lunar limb; (f) the NEC (New Extended Control) points are located in the nadir region of the photographs.

Identifying known control positions on the Apollo 15 film proved to be a time consuming task. The enhanced Orbiter IV photographs of the front side with the ACIC control points identified were examined and one control point was found. Three other control points were found from the pictures of the Lunar Landmark Control features. This is a most important network of control. It encircles the lunar equator and was established by reductions of numerous sightings of features by orbiting Apollo astronauts. Without this control network the project of extending control photogrammetrically
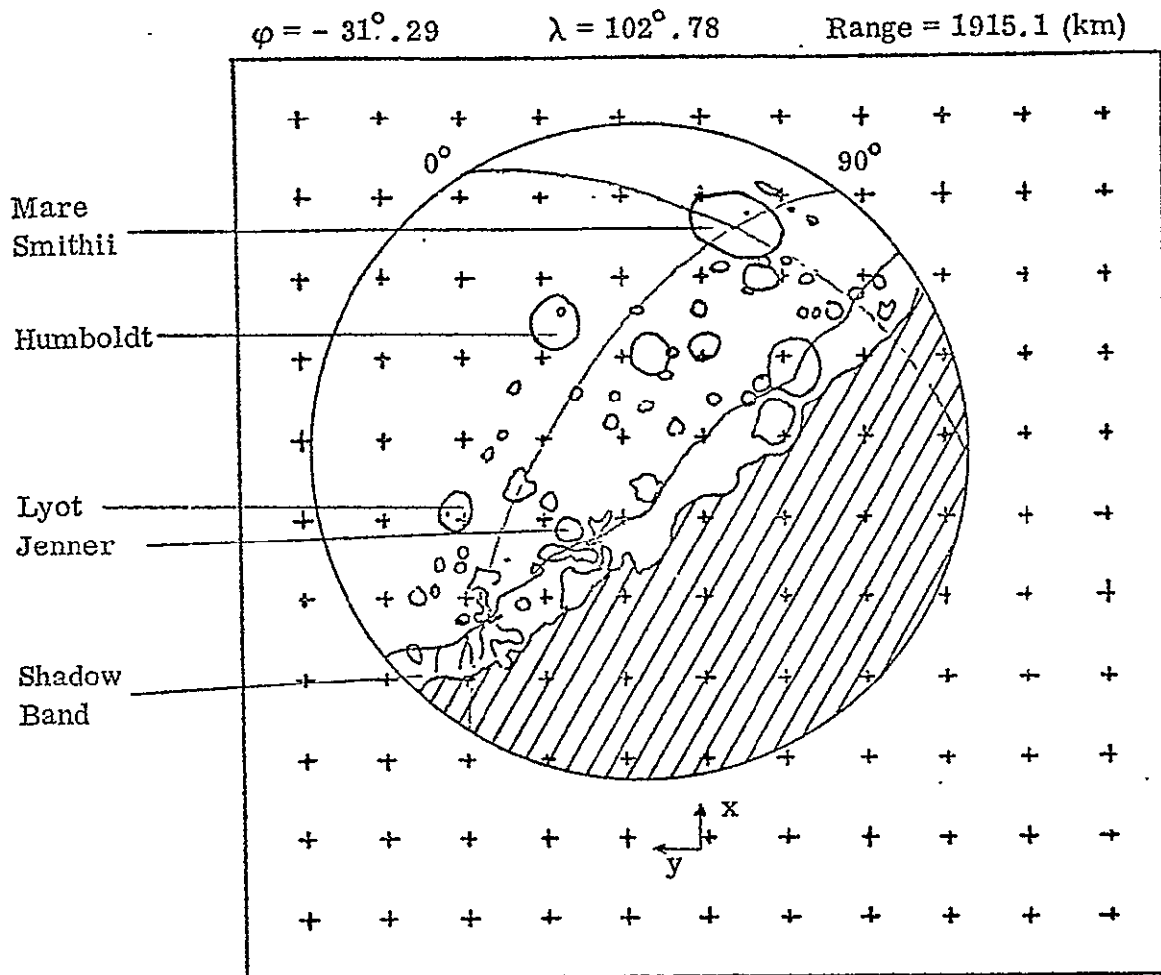
Fig. 3.1-2   Frame 2780 at TEI + 30 min.

would be seriously hampered.

Seven NEC points were selected as the points for which improved coordinates were desired. These are relatively small craters; however, they should be easily identifiable on pictures taken of the same area on succeeding missions.

These eleven points on twelve photos were measured on a first-order instrument, an AP/C (Analytical Plotter/Commercial). The least squares reduction of the measurements to the photo system contained the computation for radial distortion. The radial distortion ranged from 0.8 µm to 44.4 µm

and averaged 15.48 μm. This is within the range established in the camera specifications.

These reduced observations of visible features, the calibrated focal length, the estimated values of the selenographic coordinates for each control and NEC parameter, the estimated values of the elements of exterior orientation parameters and the weights for the photo observations and estimated parameters formed the input to the FORTBLOCK adjustment program. The FORTBLOCK adjustment triangulation program performed a simultaneous least squares adjustment on the estimated parameters (i.e., elements of exterior orientation and lunar coordinates) based on the above inputs and the collinearity condition.

The block adjustment was processed in 6 and 12 photo blocks. The program normally iterates internally three times; however, due to the unusual conditions of receding photography, the 6 and 12 photo blocks were iterated three times and then also for an additional three times. Table 3.1-3 shows the summary of the adjustment with the smallest standard deviations for the NEC points for the 12 photo block with six iterations. The adjusted values for the NEC points were then processed to provide the adjusted latitude, longitude and heights above or below a sphere of 1738.1077 km radius.

In summary (a) the standard deviations of the NEC points decrease as the number of photos and iterations are processed in the adjustment. The small differences in the standard deviations indicate the solution has reached its limitation with the six iterations of the 12 photo block.

(b) The standard deviation for the Y coordinate for NEC points 12-17 which are located near the nadir region of the photograph are always

Table 3.1-3

Summary of Results 12 Photo Block Adjustment (6 Iterations)

NEC Point No.	No. of Photos App. On	Adjusted Values of Survey Coordinates (km)			Residuals (km)			Standard Deviation (km)		
		X_a	Y_a	Z_a	v_x	y_y	z_z	σ_x	σ_y	σ_z
11	12	− 100.378	1723.743	− 133.725	− 1.879	7.369	− .121	.538	.810	.928
12	8	− 152.632	1438.456	− 950.355	− 6.400	3.450	− 9.471	1.291	2.529	1.558
13	12	− 119.109	1306.499	− 1132.546	− 5.609	− 11.190	− 15.110	1.389	2.922	1.757
14	12	123.220	1327.734	− 1104.417	2.454	4.409	− 6.331	1.494	2.694	1.526
15	12	154.426	1083.855	− 1347.756	− 4.039	4.989	.320	1.611	3.602	2.223
16	8	− 1.244	970.962	− 1439.079	− 8.006	− 3.084	− 5.761	1.632	4.253	2.658
17	6	− 224.673	1373.941	− 1028.307	2.055	− 1.446	− 1.336	1.311	2.852	1.753

$\sigma_0 = 1.56$

Average $\rho_{xy} = - .07504$

Average $\rho_{xz} = - .14994$

Average $\rho_{yz} = - .57366$

greater than the standard deviation of X or Z. The correlation coefficients ρ_{xy} and ρ_{yz} were greater than ρ_{xz} and also these NEC points are relatively highly correlated with each other. This can be attributed to the poor geometry of intersecting rays to points near the center of the photograph and also because all the photographs were taken with the selenographic Y axis nominally toward the spacecraft, thus the convergence is not as precise as in the X-Z direction.

(c) The adjustment of the 6 and 12 photo block had an effect on the residuals and standard deviations of the four control points. In almost all cases the resulting standard deviations increased slightly from the values provided by NASA. It is felt that the unique geometry not only from the spacecraft traversing away from the lunar surface but also the location of the control in just the northern limb of the photographed moon creating a very narrow cone of intersecting rays contributed to this problem.

3.14 Conclusions and Recommendations

The results show that the system originally specified in theory [Sprague, 1971] is workable with real data. The location of relatively unknown features on the lunar limb can be improved from 20 km to 1-3 km by use of photogrammetric procedures with metric film taken on one Apollo trans-earth trajectory. As a result of the investigation (a) it was recommended that the same project be accomplished using the data and film from Apollo 15, 16 and 17. The solution using photographs of the same area from different post-TEI trajectories will provide improved solutions through additional perspective rays.

59

(b) The TEI trajectories should be aligned in a more equatorial region. This would allow all the control points within the region to be observed and measured and would allow all the control points to appear in the central region of the photographed moon.

(c) The Lunar Landmark Control network should be densified with additional sightings on succeeding Apollo missions. Improved solutions of extension of control problems using photogrammetry can be provided when additional control is available.

3.2 Lunar Near-Side Positions from Earth-Based Photography

H.B. Papo[1]

3.21 Introduction

The problem to be treated in this paper can be defined broadly as
mapping the moon. By mapping the moon we mean here the determination of
positions of specific points and features on its surface relative to a
certain coordinate system. Coordinate systems can be chosen at will, but
there is added importance to those which are physically significant. For
the moon a Cartesian coordinate system can be defined which is centered at
its mass center and is oriented along its three principal axes of inertia.
The above system will be referred to as the selenodetic coordinate system
of the moon.

There are in existence many different maps of the moon which define
coordinates of features on its surface. Unfortunately, the same features
have different coordinates on different maps. The main reason for these
differences is the lack of a unique fundamental control network on the moon.
A network of 20 or 30 distinct features on the visible side of the moon
which have precise coordinates with respect to the selenodetic coordinate
system could serve as fundamental control on the moon. In order to avoid
the large discrepancies between the various maps, any subsequent densifica-
tion of control for mapping purposes should be derived from the same
fundamental control points. Thus the specific problem to be treated in

---

[1] Presently at the Technion, Haifa, Israel.

this paper is the establishment of a <u>fundamental selenodetic control network</u> on the moon.

A basic difference between the earth and the moon in establishing such a control system is in the fact that there are no observations of geodetic significance which have been performed from the lunar surface. On earth we use classical or satellite triangulation and trilateration geodetic astronomy and gravimetry in all of which the observations are conducted from points on the earth's surface. On the moon such an analogy is still nonexistent. The only observational material at our disposal are remote observations taken directly from the earth's surface or indirectly from a spacecraft which is tracked continuously from earth. Because of this important difference, establishing control on the moon is inseparable from two aspects of its motion in space, namely, the instantaneous <u>position of the center of mass</u> of the moon with respect to the earth and the instantaneous <u>orientation of the selenodetic coordinate system</u> with respect to inertial space. These two aspects are by themselves rather difficult problems in dynamical astronomy; however, there is no way of establishing a control of physical significance without insuring its <u>consistency with the motion of the moon.</u>

The numerical lunar ephemeris introduced by the Jet Propulsion Laboratory under the code name LE-16 represents the translatory motion of the lunar mass center with respect to the geocentric 1950 mean equatorial coordinate system. According to the definition given above, the instantaneous position of the origin of the selenodetic coordinate system at a specific epoch is identified in our study with the LE-16 lunar ephemeris.

The second aspect of the motion of the moon, namely, its rotation

about an axis passing through its mass center, was made an integral part of our solution for fundamental control. At any specific epoch the rotation of the moon defines the instantaneous orientation of the selenodetic coordinate system with respect to inertial space. In our study the parameters of orientation of the selenodetic system are identified with the physical libration of the moon. A full account on the approach taken in solving the physical librations of the moon is given in section 2.2.

The solution for fundamental control presented in this paper is based on remote optical observations of the lunar surface. Photography of the moon taken from the earth or from satellite-borne cameras as well as direct angular observations to specific features on the moon taken from the earth or from a satellite all form the main bulk of observational data. Auxiliary data designed to provide orientation and scale to the optical data is also considered (stellar camera, star background lunar photography, etc.).

Another important although "nonoptical" auxiliary data source are range-rate observations from the earth to a spacecraft involved in optical observations of the moon. As the instantaneous position of the spacecraft with respect to the moon at any specific epoch is derived from analysis of range-rate observations, this data is also processed in the general solution for fundamental control.

3.22 Basic Concepts

For a fundamental orientation frame of reference, a hypothetical inertial coordinate system is considered which coincides with the ecliptic mean coordinate system at some arbitrary standard epoch and is defined as a Newtonian Frame of Reference [Brouwer and Clemence, 1961, p. 3]. The orientation of any other Cartesian coordinate system with respect to the

63

inertial system is defined through three Eulerian angles necessary to rotate the particular Cartesian system into the inertial or vice versa (see Fig. 3.2-1). The term inertial coordinate system, to be denoted by XYZ, is used for any coordinate system (having an arbitrary origin) which is parallel to the fundamental orientation frame. Thus, one may have a geocentric inertial system, an inertial system centered at a satellite, etc.

The orientation of a physical body is defined through a Cartesian coordinate system fixed to the body. Thus, for example, the orientation of the earth is defined through the so-called average terrestrial coordinate system which is fixed to the earth's crust and related to a geocentric inertial system by means of three Eulerian angles.

There are three Cartesian systems which are of primary importance:

(a) The average terrestrial system is centered at the mass center of the earth and is oriented with respect to the crust through the CIO pole and the so-called mean observatory [Mueller, 1969]. It is denoted by UVW.

(b) The selenodetic system is centered at the mass center of the and is oriented along its principal axes. It is denoted by xyz.

(c) The optical observations reference system is centered at the projection center (from which the optical rays emanate) and is generally oriented so that the primary axis (B_1) points towards the moon. It is denoted by $B_1B_2B_3$.

The general rotational motion of a physical body with respect to the inertial system is described by the change with time in the Eulerian orientation angles of the appropriate coordinate system (the one fixed to the body).
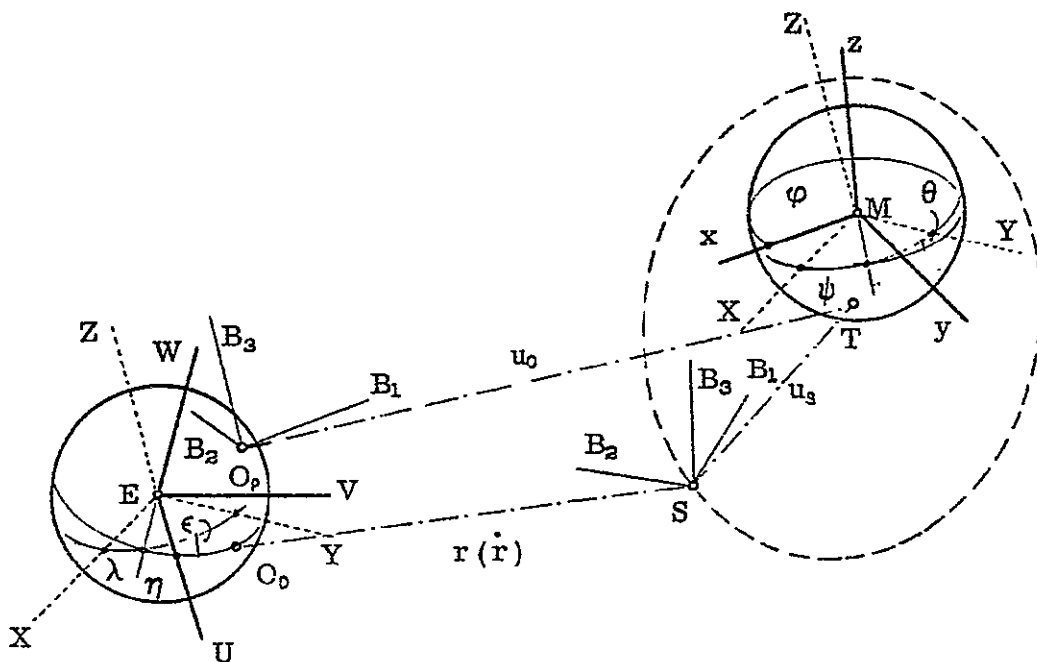
Fig. 3.2-1 Earth-moon environment.

E	-	the geocenter
M	-	the selenocenter
S	-	a satellite
XYZ	-	inertial coordinate systems
UVW	-	average terrestrial coordinate system
xyz	-	selenodetic coordinate system
$B_1B_2B_3$	-	reference frames for optical observations
η, λ, ϵ	-	Eulerian orientation angles of the Earth
φ, ψ, θ	-	Eulerian orientation angles of the Moon
O_P	-	observing station for optical observations
O_D	-	tracking station for range and range rate observations
T	-	triangulation point on the Moon
$r\,(\dot{r})$	-	range (range rate) between O_D and S
$\left.\begin{array}{c} u_O \\ \\ u_S \end{array}\right\}$	-	optical ray (direction) between O_P or S and T.

65

Thus, for example, in order to study the rotational motion of the moon one should consider the changes in the Eulerian angles (ϕ, ψ, θ) which relate the oon-fixed (xyz) system to the inertial (XYZ) system. From this definition of rotational motion it is clear how rotation and orientation of a body are related to one another. As the body rotates, its orientation changes and by considering the instantaneous set of Eulerian angles at a particular epoch one has the means for defining the orientation of the body at that epoch.

The rotation of a physical body is governed by a set of equations of rotational motion (second-order differential equations) in which the external forces acting on the body are represented. The solution of these equations of motion results in the Eulerian orientation angles as functions of time.

The position with respect to the UVW system of points on the surface of the earth is defined similarly with respect to the selenodetic (xyz) system.

The position and velocity (state vector) of points in space with respect to a particular inertial coordinate system (selenocentric, geocentric, etc.) are defined by Cartesian coordinates (XYZ). Thus, the geocentric state vector of the moon's mass center is given by the LE-16 ephemeris [O'Handley et al., 1969] where the inertial XYZ system has been defined as identical to the mean equatorial system of 1950.0.

All optical observations of the moon (photographs, direction measurements, etc.) are treated as light rays emanating from a projection center whose selenocentric inertial coordinates are known or are being estimated in a least squares process. The individual ray from a bundle (the rays

emanating from the same projection center form a bundle) is related to a reference optical frame $B_1B_2B_3$ by two angular quantities. As mentioned above, the $B_1B_2B_3$ is related to the XYZ system centered at the projection center by three Eulerian angles or in general by an orthogonal transformation matrix.

If the projection center is on board a spacecraft, range and range-rate data from the earth to the spacecraft serve for determining its selenocentric orbit. The ordinary orbit determination procedure solves for the state vector (position and velocity) at a standard (initial) epoch as well as for a number of constants. As some of these constants are dominant factors in the rotational motion of the moon and also as the projection center from which the optical observations are made lies along the trajectory of the spacecraft, it is necessary to process the range and range-rate tracking data together with the optical data and thus obtain a solution for the trajectory and for the relevant constants which is consistent with both types of data.

To summarize, the moon is regarded as a rigid celestial body rotating in space under the gravitational influence of the earth and the sun while around it there is a variety of sensors engaged in optical observations. The optical observations as well as the range-rate and other auxiliary data are modeled into observation equations in terms of the parameters of the solution and are treated thereafter by a weighted least squares procedure.

3.23 Adjustment Theory

The mathematical model for an optical observation is derived from the triangle formed by the selenocenter M, the particular control point being observed T and the projection center S or 0_p (see Fig. 3.2-1).
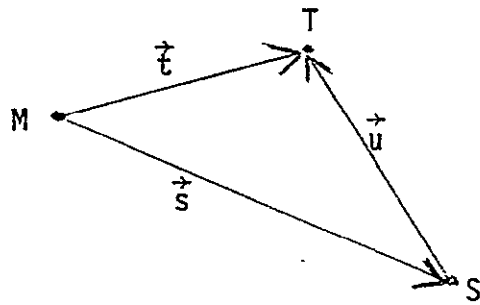
Fig. 3.2-2

If we denote the vectors connecting the three vertices M,T,S according
to Fig. 3.2-2, the mathematical model simply is

$$F = \vec{u} + \vec{s} - \vec{t} = 0$$

where

$\vec{u}$ represents the optical observation

$\vec{t}, \vec{s}$ represent the selenocentric position of the control point and the

projection center respectively.

The mathematical model for range-rate observations is derived from the
triangle defined by M, as before, the spacecraft S and the tracking station
on earth O (see Fig. 3.2-3).
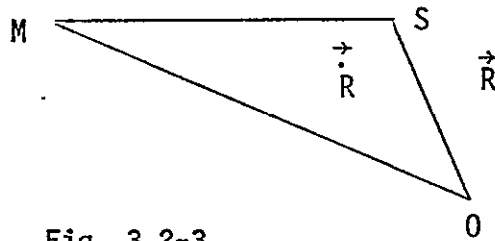
Fig. 3.2-3

If $\vec{R}$ denotes the instantaneous position of S with respect to O and $\dot{\vec{R}}$ is the
corresponding time derivative of $\vec{R}$, the following equation holds:

$$H = \frac{1}{|\vec{r}|} (\dot{\vec{R}} \cdot \vec{R}) - |\dot{r}|^b = 0$$

where r is the range (distance) $\overline{OS}$ and $\dot{r}$ is the observed rate of change of r.

68

The above nonlinear models have to be linearized before an adjustment procedure can be developed. By linearization we mean the usual Taylor expansion of the models in terms of small corrections to the approximate values of the parameters. The parameters considered in the adjustment are of two basic types, namely, parameters which are being sought to be referred to as permanent and parameters which are not of interest but which are indispensable in modeling the observations. The permanent parameters of the solution are placed into three groups:

(1) Cartesian coordinates of the control points (3 x n)

(2) parameters of orientation of the moon (6)

(3) selected physical parameters of the moon (3).

If we choose to limit the number of control points to say 22, the total number of unknowns would be 75 which is not too large for a simultaneous solution on a medium size computer. The situation is enhanced further by the fact that the normal equations can be created by the summation of individual layers. The final set of the 75 normal equations is obtained by sequential addition of the contribution of numerous batches of optical observations. In this way the maximum size of the computer program required to form and solve the normal equations is determined mainly by the number of control points and not be the number of observations which in our case may run into the thousands.

As the physical librations form an integral part in the solution, the particular logic of the adjustment procedure was developed with the numerical integration program for the physical librations serving as a backbone. The sequence of steps is as follows:

(1) The integrating program is operated up to the "next" epoch at which

a bundle was observed.

(2) The integration is arrested and the information generated by the
integrating program for that epoch (physical libration angles, state
transition and parameter sensitivity matrices) together with informa-
tion gathered by the optical bundle are used in evaluating the partial
derivatives as developed in [Papo, 1971, section 2.4].

(3) A layer of the normal matrix, the constant vector and the considered
parameters contribution matrix is generated and added to the corres-
ponding matrices where layers from previous bundles have been
accumulated.

(4) The integration is resumed until the epoch of the "next" bundle and so
on, until all the bundles in the batch have been processed. It should
be remembered that the normal matrix generated is that of the permanent
parameters only, the solution for the auxiliary parameters being
"folded in."

(5) The a priori covariances of the permanent parameters are added to the
normal matrix followed by inversion and subsequent evaluation of the
solution vector (corrections to the starting values of the permanent
parameters) and the full covariance matrix of the corrected (adjusted)
parameters.

The above procedure is used for processing earth-based optical observations.
Processing satellite-based optical observations is done in a similar way only
now the range-rate data is added in the process and also the number of
auxiliary (nonpermanent) parameters is increased to allow for the orbit
determination of the satellite.

70

3.24 Numerical Experiments

In order to test numerically the mathematical procedure developed in this study, a simulated environment was created which reflects very closely the true world. The earth, the moon and a variety of satellites move and rotate in this simulated environment strictly according to the laws of Newton and Kepler.

The solution as proposed was tested through the analysis of simulated optical observations. The observational material was generated free of any unaccounted phenomena and simulated very closely real observations.

Thirty well distributed points on the front side of the moon were chosen as the control network and over a period of one year thirty simulated photographs (bundles of optical rays) were taken from observatories on earth (see Fig. 3.2-4). Solutions were performed varying the accuracy of the observational material and also varying the initial (approximate) values of the parameters.
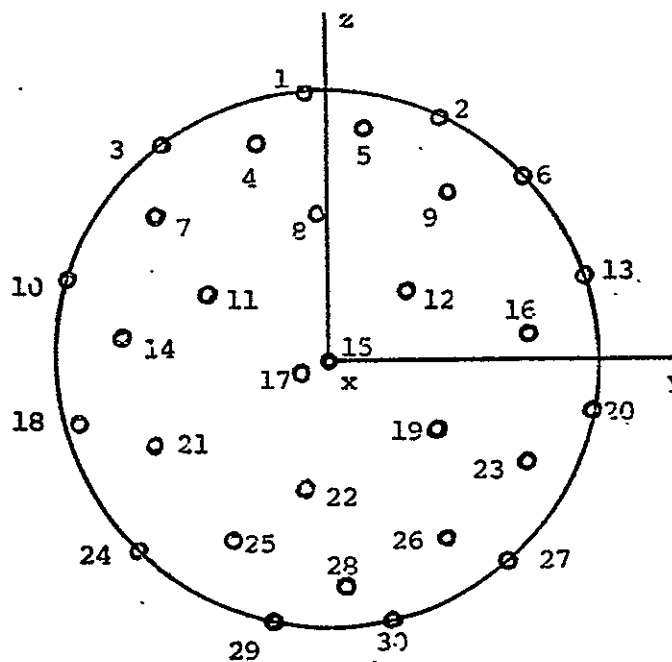

Fig. 3.2-4 Fundamental control network.

71

The objectives of the experiment were twofold:

(1) To determine the quality of control solution which can be obtained from the simulated observational material. This was done by inspecting the covariance matrix of the solution vector of the parameters.

(2) To find to what extent the adjustment procedure is capable of recovering shifts which were introduced in the nominal values of the parameters. This was accomplished by using the shifted values as first approximations in the adjustment and by subsequent inspection of the solution vector.

Table 3.2-1 presents diagonal submatrices of the covariance matrix of the solution for control coordinates in kilometers squared. It also gives the corresponding correlations. A clear pattern of higher correlations can be observed as follows: the x coordinates are correlated among themselves and the same applies to the y and z coordinates respectively. A possible reason for this phenomena may be that the orientation of the moon was made a part of the solution. Typical for all the points is that the x coordinates are determined much less accurately as compared to the y and z coordinates. The main reason for the apparent deficiency in determining the x coordinates is undoubtedly the poor geometry of any optical observation of the moon as taken from the earth. We should realize that the maximum angle of convergence between optical rays from different bundles is usually much less than 23 degrees (see Fig. 3.2-5). The average standard deviations for x, y and z are 700, 150 and 150 m.

Table 3.2-2 presents the correct coordinates (nominal) of the control points and the negative values of the solution vector after one iteration

Table 3.2-1

Covariance and Correlation Matrices for Solution of Network I
from 30 Bundles. Triangulation Points.

Control Point Nos.
☐ 11, 12, 13
☐ 17, 18, 19
27, 28, 29 ☐

Covariance Matrix in km²
Correlation Matrix
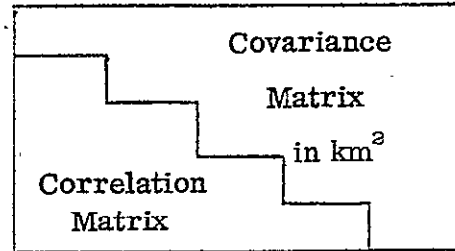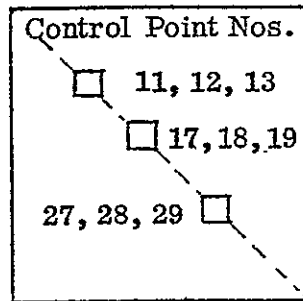
Parts of Covariance/Correlation Matrix on this Page

	11			12			13		
0.483	0.CC9	-0.001	0.303	0.009	-0.000	-0.271	-0.0C1	-0.001	
0.061	0.047	0.000	-0.019	0.046	0.000	-0.037	0.018	0.0C1	11
-0.008	-0.001	-0.015	-0.001	-0.000	-0.012	0.001	-0.000	-0.010	
0.624	-0.128	0.016	0.488	-C.023	-0.001	0.309	-0.007	-0.003	
0.060	-0.953	C.0C2	-0.146	-0.050	C.000	-0.039	C.C19	-0.001	12
-0.004	0.018	0.818	-0.009	0.018	0.014	-0.001	C.000	0.011	
-0.529	-0.229	C.0C8	-0.600	-C.238	-0.012	0.544	-0.012	-0.002	
-0.C09	0.679	0.025	-0.077	C.669	0.015	-0.135	0.015	-0.000	13
-0.008	-0.023	0.664	-0.031	0.022	-0.755	-0.023	-0.010	-0.015	
x	y	z	x	y	z	x	y	z	

	17			18			19		
C.480	-0.007	-0.001	0.283	-0.002	-0.002	0.309	-0.007	-0.001	
-0.044	0.058	-C.000	0.040	0.023	-0.0C1	-0.027	0.050	0.C00	17
-0.014	-0.002	-0.014	-0.001	-0.000	-0.012	-0.002	-0.000	-0.012	
C.551	0.226	-0.013	C.551	C.CC8	-0.005	0.261	0.035	0.000	
-0.022	0.740	-0.013	-0.083	-0.017	-0.000	-0.CC8	C.C22	-0.000	18
0.028	-0.033	0.818	-C.059	-0.030	0.016	0.004	-0.001	0.011	
0.639	-0.162	0.024	0.505	-0.CE7	0.041	0.485	-0.027	-0.000	
-0.045	0.954	-0.012	0.214	0.765	-0.045	-0.177	0.047	0.C00	19
-0.008	0.017	C.822	0.005	0.006	0.780	0.006	0.014	-0.014	
x	y	z	x	y	z	x	y	z	

	27			28			29		
0.490	-0.013	-C.0CC	0.300	-0.019	0.001	0.294	-0.010	0.002	
-0.144	0.017	0.001	-0.005	0.018	-0.000	-0.000	0.015	-0.000	27
-C.CC5	0.042	0.014	-0.000	0.001	-0.011	-0.000	-0.001	0.011	
0.629	-0.059	-0.0C3	0.466	-0.007	0.002	0.297	-0.CC4	0.002	
-0.161	-0.840	-0.046	-0.062	-0.028	-C.000	-0.004	0.018	-0.001	28
C.C17	-0.020	C.800	0.025	-0.017	0.014	0.001	-0.000	0.011	
0.604	-0.003	C.0C6	0.625	0.C34	-C.014	C.484	-0.001	0.C01	
-0.1C6	0.859	0.049	-0.048	0.813	-0.026	-C.010	0.017	-0.001	29
0.021	-0.028	C.755	0.020	-0.C28	-C.828	-0.0C9	-0.033	0.014	

73

Table 3.2-2

Solution Vector for Test (a) in Experiment (ii)

Solution Vector

	x	y	z	x	y	z	
1	-0.249195D 00	0.810167D 00	-0.671682D 00	0.451232D-01	-0.509060CD 00	-0.164511D 00	2
3	-0.487323D 00	0.439074D 00	-0.263503D 00	-0.341844D 00	-0.540649D 00	-0.197584D 00	5
6	0.339017D 00	-0.354513D 00	-0.734539D 00	-0.124563D 00	0.594323D 00	-0.688796D 00	7
8	0.213988D 00	0.276810D 00	-0.139755D 00	0.216075D 00	0.904401D 00	-0.600756D 00	10
11	-0.289036D-01	0.846637D 00	-0.485766D 00	0.171767D 00	-0.963741D 00	-0.583646D 00	12
13	0.216689D 00	-0.928099D 00	-0.601710D 00	0.872806D-01	-0.132957D-01	-0.830196D 00	15
17	-0.167222D 00	0.264872D 00	0.468104C 00	-0.128061D 00	0.775267D 00	0.987563D 00	18
19	0.228009D 00	-0.433069D 00	0.590006D 00	-0.258044D 00	-0.710317D 00	0.321186D 00	20
22	-0.424128D 00	0.478941D 00	0.155174D 00	-0.936816D-02	0.954561D 00	0.893347D 00	24
27	-0.331822D 00	-0.486726D 00	0.792996C 00	-0.949658D-01	-0.517581D 00	0.204517D 00	28
29	0.129645D 00	0.777090D 00	0.543599D 00	-0.154755D-01	-0.153719D-01	0.280252D 00	30
T	-0.122154D 00	0.549717D-02	-0.625151D-01	-0.267345D-03	-0.185167D-01	-0.503032D-02	
C_{aa}	-0.225211D-02	-0.193683D-01	-0.900843D-07	C_{ab}	t	σ	ρ

Absolute (Simulated) Coordinates of Triangulation Points

|	x	y	z	x	y	z	
1	284.7144	-164.8233	1705.6738	267.3828	742.4968	1548.1653	2
3	298.9905	-1050.4536	1350.2634	897.8094	293.5282	1457.1998	5
6	297.0151	1208.3423	1116.7341	1013.5746	-1088.6066	894.6916	7
8	1453.2070	-75.2901	946.1413	341.1861	-1615.9158	536.6048	10
11	1506.4731	-767.8602	390.4892	1577.2501	544.9516	478.5874	12
13	341.1861	1617.9158	536.6048	1735.3430	1.	29.8342	15
17	1726.6207	-150.2785	-91.4655	490.5786	-1611.7874	-420.9863	18
19	1499.1838	732.4201	-479.5874	294.7339	1686.6973	-302.3192	20
22	1511.8985	-131.4927	-843.1513	257.4499	-1221.9682	-1207.8911	24
27	449.7967	1120.4735	-1250.7900	940.5390	83.5052	-1458.1998	28
29	377.2905	-378.7905	-1653.5386	305.4515	368.0022	-1671.2764	30

74
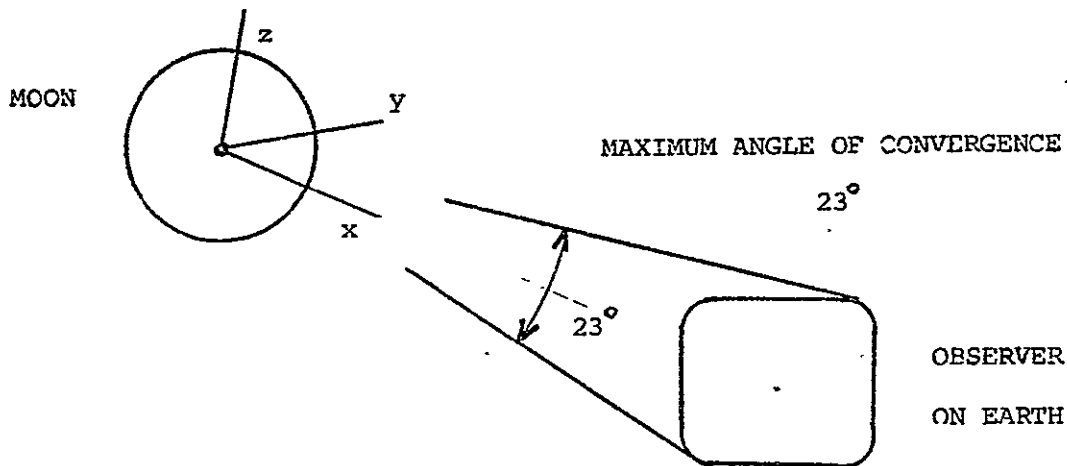
Fig. 3.2-5 From the earth the moon is seen through a
narrow window.

of the adjustment. The shifts in the coordinates were obtained by simply

removing the decimal fraction of the coordinates. So the degree of recovery

of the shifts is within 10-20 m in y and z which is remarkable considering

the low quality of the solution as exhibited by the covariances. As could

be expected after only one iteration, the recovery in x is much less

efficient.

3.25 Summary

The main characteristics of the solution for selenodetic control as

developed in this study are summarized in the following:

(a) The solution is consistent with the motion of the moon in space.

(b) The solution for the orientation of the moon in space is part of

the general solution.

(c) Optical data obtained from the earth or from a spacecraft are

processed uniformly, thus avoiding inconsistencies between solutions based

on either of the two sources of data.

(d) All the observations needed for the solution (optical, range, and

range-rate) are processed simultaneously in a weighted least squares

75

procedure where the parameters are constrained according to their a priori covariances.

(e) The adjustment procedure can be programmed for used with available electronic computers where the core size required and the computer time for processing the data are reasonable and make the application of the solution to processing real data a feasible proposition.

3.3 Positioning from Lunar Laser Ranging

F. Fajemirokun[1] and F. Hotter

3.31 Introduction

Lunar laser ranging has provided another means by which geodetic control can be established on the moon. It is now estimated that distances between stations on the earth and lunar retroreflectors can be measured with a precision of ±15 cm with laser techniques [Alley et al., 1970]. An improvement in this precision is expected in the future.

As opposed to the methods of establishing geodetic control for earth mapping which involve measurements on the earth's surface itself, past selenodetic controls have been obtained mainly through the use of earth-based or lunar satellite-based observations. Thus, the determination of coordinates of points on the moon through these methods is rigorously tied to the following extraneous parameters:

(1) the coordinates of the moon's center of mass in a geocentric inertial coordinate system,

(2) the orientation parameters of an earth-fixed coordinate system with respect to a moon-fixed coordinate system,

(3) parameters of the atmospheric refraction model used when reducing the earth-based observations.

Lunar laser ranges of such precision, as mentioned above, expected not only to improve the accuracy of positions of points on the moon, but also to

---

[1] Presently at the University of Lagos, Lagos, Nigeria

contribute to more accurate determination of the geocentric positions of laser stations on the earth. Furthermore, it is expected that the parameters of the earth's and moon's orientation in space can be also improved upon.

The relative position of a lunar point (such as the retroreflector) with respect to a station on the earth depends on a number of physical and geometric parameters of the earth, moon and the earth-moon dynamic system. Therefore, a measured distance between an earth station and a lunar point can be expressed mathematically as a function of the following parameters:

    a.   the selenodetic coordinates of the lunar point,

    b.   the geocentric coordinates of the center of the moon,

    c.   the geodetic coordinates o f the earth station,

    d.   parameters of the orientation of a moon-fixed coordinate system with respect to a celestial coordinate system,

    e.   parameters defining the orientation of the "average" terrestrial (earth-fixed) coordinate system with respect to the celestial coordinate system.

Before deriving the earth-moon distance equations, the above-mentioned coordinate systems and orientation parameters will be given brief descriptions:

The selenodetic coordinates--longitude ℓ, latitude b, and radius r-- define conventionally the location of a point on the lunar surface. The selenodetic latitude is measured from the lunar equator positive toward the north lunar pole. The prime meridian ($\ell = 0$) is a plane which contains the lunar axis of rotation and the earth-moon line at zero geometric libration. The longitude is measured from this prime meridian positive in the direction of rotation. The Cartesian selenodetic coordinate system

(x,y,z) is fixed with respect to the solid moon, is centered at the moon's center of mass (selenocenter) and is related to the coordinates ℓ, b, and r the usual way [Mueller, 1969].

The geocentric coordinates of the selenocenter is obtained from a lunar ephemeris based on a particular lunar theory which attempts to solve the differential equations of motion of a perturbed two-body system. These differential equations can be integrated either analytically [Brown, 1908] or numerically [O'Handley et al., 1969].

The "average" terrestrial coordinate system (u,v,w) in which coordinates of the earth stations are expressed is defined by the Conventional International Origin (w-axis) and the Greenwich Mean Astronomical Meridian as determined by the Bureau International de l'Heure (u-axis) [Mueller, 1969]. The coordinate system is fixed to the solid earth and is centered at its center of mass. The Cartesian coordinates (u,v,w) can be computed from the conventional geodetic latitude (ℓ), longitude (λ) and height (h) the customary way [Mueller, 1969].

3.32 Numerical Experiments

Numerical experiments were performed for the purpose of investigating the expected accuracies of the parameters in the adjustment model using laser observations of currently expected precision. Since no real data were available, laser distances were simulated for the purpose of these experiments.

The numerical experiment utilized the three lunar retroreflectors so far deposited on the moon in the Apollo program, to which distances were simulated from certain existing laser stations on the earth. First, a set of experiments were performed using only the laser station at the

McDonald Observatory ranging to the three retroreflectors. Later, in order to find out the effect of multiple observing stations on the recovery of the parameters, two stations were added: Mt. Stromlo and the Crimean Observatories. Tables 3.3-1 and 3.3-2 contain the coordinates of the laser stations and the lunar retroreflectors.

For the limited objectives of these experiments, only the following parameters were included in the adjustment as unknowns:

(1) The geocentric (u,v,w) coordinates of the laser stations on the earth.

(2) The six parameters of the orientation of the (u,v,w) "average" terrestrial coordinate system with respect to the mean ecliptic coordinate system of 1969.0. These are the Eulerian angles and their time derivatives for the epoch of 1969.0. (θ,ψ,Φ).

(3) The selenodetic (x,y,z) coordinates of the lunar retroreflectors.

(4) The parameters of the orientation of the (x,y,z) lunar coordinate system with respect to the mean ecliptic system of 1969.0, represented by the physical libration parameters--τ,σ,ρ--and their derivatives at the epoch of 1969.0.

(5) Three physical parameters of the moon given by the spherical harmonic coefficients C_{20}, C_{22} and the moment of inertia ratio $\beta = \frac{C - A}{B}$.

The simulated data were assumed to be completely free of systematic errors, and the geocentric coordinates of the moon's center of mass were assumed to be correct as given in the ephemeris [O'Handley et al., 1969].

The numerical integration of the earth's Eulerian angles is outlined

80

Table 3.3-1

Geocentric Coordinates of Laser Stations

Point No.	u(km)	v (km)	w(km)	Location
1	-1330.81462	-5328.78935	3235.69752	Ft. Davis, Texas
2	-4466.54586	2683.24104	-3667.44266	Mt. Stromlo, Australia
3	3784.28692	2552.21344	4440.46175	Crimean, USSR

Table 3.3-2

Selenodetic Coordinates of Lunar Retroreflectors

Point No.	x(km)	y(km)	z(km)	Remarks
1	1591.42945	691.97322	19.26380	Apollo 11 Mission
2	1652.86823	-520.44969	-110.54128	Apollo 14 Mission
3	1554.85951	99.26753	762.35841	Apollo 15 Mission

in [Fajemirokun, 1971]. In the Encke-type of integration, the quantities integrated are the following:

$$
\begin{vmatrix} \delta_1 \\ \delta_2 \\ \delta_3 \\ \delta_4 \\ \delta_5 \\ \delta_6 \end{vmatrix} = \begin{vmatrix} \theta - \theta_C \\ \psi - \psi_C \\ \Phi + \psi - K_0 - K_1 t \\ \dot\theta \\ \dot\psi \\ \dot\Phi + \dot\psi - K_1 \end{vmatrix}
$$

where θ_C, ψ_C, K_0 and K_1 are constants. The expression for the state transition matrix U, which was obtained by numerical differentiation is given as

$$ U = \frac{\partial \delta}{\partial \delta_0} $$

where

$$ \delta = [\delta_1 \; \delta_2 \; \delta_3 \; \delta_4 \; \delta_5 \; \delta_6]^T $$

and

δ_0 is the value of δ at the initial epoch of 1969.0.

For the corresponding lunar parameters, the method described in [Papo, 1971] was used which integrates the physical libration parameters $(\tau, \sigma, \rho, \dot\tau, \dot\sigma$ and $\dot\rho)$. The Eulerian angles and their time rates were obtained from the physical libration quantities and the Cassini expressions as follows:

$$
\begin{vmatrix} \Phi \\ \psi \\ \theta \\ \dot\Phi \\ \dot\psi \\ \dot\theta \end{vmatrix} = \begin{vmatrix} L + \Pi - \Omega \\ \Omega \\ I \\ \dot L - \dot\Omega \\ \dot\Omega \\ 0 \end{vmatrix} + \begin{vmatrix} \tau - \sigma \\ \sigma \\ \rho \\ \dot\tau - \dot\sigma \\ \dot\sigma \\ \dot\rho \end{vmatrix}
$$

where

L is the mean longitude of the moon in its orbit

Ω is the longitude of the mean ascending node of the moon's orbit

I is the mean inclination of the lunar equator with respect to the ecliptic

In addition to the physical libration quantities and the state transition matrix, the integration program also computes the parameter sensitivity matrix

$$S = \frac{\partial [\tau \; \sigma \; \rho \; \dot{\tau} \; \dot{\sigma} \; \dot{\rho}]^T}{\partial [C_{22} \; \beta \; C_{20}]^T}$$

and the state transition matrix

$$U^* = \frac{\partial [\tau \; \sigma \; \rho \; \dot{\tau} \; \dot{\sigma} \; \dot{\rho}]^T}{\partial [\tau_0 \sigma_0 \rho_0 \dot{\tau}_0 \dot{\sigma}_0 \dot{\rho}_0]^T}$$

The adjustment method regards all the parameters (in addition to the simulated distances) as observations with associated weights. The relative weights of the parameters were computed as the inverse of their estimated variances, thereby choosing the variance of unit weight to be equal to one.

The values of the variances of parameters were selected to conform with the level of uncertainties in the present knowledge of these quantities. The chosen standard deviations of the parameters are given in the last column of Table 3.3-3.

3.33 Results

The purpose of this experiment was to investigate the internal precision of the adjustment system. There were three cases investigated:

83

(1) Laser distances were simulated between McDonald Observatory and the three lunar retroreflectors. The number and period of observations chosen were as follows: 50 observations over a three-month period, 100 observations over a six-month period, 150 observations over a nine-month period, and 200 observations over one year.

(2) The number of observations was held to 50 and 100 while the period of observations was varied.

(3) The simulated distances used for the adjustments comprised of distances between all the three laser stations and retroreflectors. Number and period of observations chosen were the same as in (1).

Table 3.3-3 gives the diagonal elements of the variance-covariance matrix for case (1). The general pattern shows, as can be expected, that the parameter variances decrease as more observations are made over longer periods of time. It can also be seen that in addition to a general improvement in lunar position, we can also expect an improvement in the determination of geocentric positions of stations on the earth's surface. A general improvement in the accuracy of determining the orientation parameters of both the earth and the moon, and the moon's lower order spherical harmonic coefficients can also be expected. Exceptions seem to be the variances of the physical libration in the node and its time derivative (σ and $\dot{\sigma}$). Even with 200 observations over a one-year period, the variance obtained for σ and $\dot{\sigma}$ are 250''7 and 29.5 sec^2/day^2, respectively, compared to the a priori values of 400'' and 100 sec^2/day^2. A good explanation for this poor determination of σ and $\dot{\sigma}$ was not found, especially since the dominant term of libration in node has a period of about one month. On the other hand, it should be borne in mind that the node itself is rather poorly defined through the intersection of two planes at an angle of only 1°5.

Table 3.3-3

Variances of Parameters for Case 1, (One Laser Station Observing,
Number and Period of Observations Varied)

Parameters	50 Observations 3 Months	100 Observations 6 Months	150 Observations 9 Months	200 Observations 12 Months	A Priori Variance
	$meter^2$	$meter^2$	$meter^2$	$meter^2$	$meter^2$
u	312.7	1.0	0.3	0.08	625
v	19.6	0.07	0.02	0.01	625
w	36.0	8.9	1.8	1.4	625
x_1	16.3	2.9	1.2	0.5	10^6
y_1	57.1	10.1	4.2	1.9	10^6
z_1	646.3	220.9	85.8	57.7	10^6
x_2	10.5	2.3	1.1	0.4	10^6
y_2	138.7	27.6	10.6	4.4	10^6
z_2	627.4	191.9	66.6	50.1	10^6
x_3	17.5	14.4	10.1	6.0	10^6
y_3	113.2	26.7	9.8	6.3	10^6
z_3	539.6	171.5	63.2	44.6	10^6
	$second^2$	$second^2$	$second^2$	$second^2$	$second^2$
δ_1	0.6×10^{-3}	0.1×10^{-3}	0.2×10^{-4}	0.1×10^{-4}	1.0
δ_2	0.3×10^{-3}	0.2×10^{-3}	0.8×10^{-4}	0.6×10^{-4}	1.0
δ_3	0.5	0.1×10^{-2}	0.3×10^{-3}	0.1×10^{-3}	1.0
τ	1.5	0.3	0.1	0.04	400
σ	397.8	382.0	318.7	250.7	400
ρ	1.4	1.2	0.8	0.4	400
C_{22}	0.3×10^{-2}	0.2×10^{-3}	0.5×10^{-4}	0.2×10^{-4}	0.25
β	0.4×10^{-3}	0.3×10^{-4}	0.8×10^{-5}	0.3×10^{-5}	4.0
C_{20}	0.1×10^{-3}	0.1×10^{-3}	0.1×10^{-3}	0.1×10^{-3}	0.1×10
	sec^2/day^2	sec^2/day^2	sec^2/day^2	sec^2/day^2	sec^2/day
$\dot{\delta}_4$	0.2×10^{-2}	0.2×10^{-3}	0.1×10^{-3}	0.8×10^{-4}	0.25
$\dot{\delta}_5$	0.6×10^{-1}	0.7×10^{-2}	0.6×10^{-3}	0.3×10^{-3}	0.25
$\dot{\delta}_6$	0.4×10^{-3}	0.5×10^{-4}	0.4×10^{-5}	0.2×10^{-5}	0.25
$\dot{\tau}$	0.8×10^{-3}	0.6×10^{-4}	0.1×10^{-4}	0.6×10^{-5}	100
$\dot{\sigma}$	98.2	81.3	55.1	29.5	100
$\dot{\rho}$	0.02	0.015	0.011	0.009	100

Another trend that could be noticed in Table 3.3-3 is that, in general, the x coordinates of the lunar reflectors were better determined than the y and especially than the z coordinates. The z-coordinates were the ones with the poorest determination. This phenomena can be explained through the fact that the ranges are likely to be more sensitive to changes in the x-coordinates of lunar stations since the x-axis is always oriented towards the earth. In this respect, it is interesting to note that from earth-based optical (photographic) observations the determination of the x-coordinates is the poorest compared to y and z [Papo, 1971]. Thus it can be expected that the combination of photographic and laser observations would yield good results in all three coordinates. This same conclusion cannot be drawn to the same degree for the geocentric coordinates of points on the earth which are likely to depend more on the geometry of the situation. However, the poorest coordinate seems to be the one parallel to the earth's rotation axis.

Table 3.3-4 displays the variances of parameters for case (2) where the number of observations were held fixed and the observation periods varied. All parameters showed sensitivity to the length of the period as can be seen from decreases in the variances of parameters when the period of observation was increased. The sharpest change in the variances occurred when the period of observation was increased from three months to six months. A further increase in the period to nine months showed a lesser decrease in the variances.

In Table 3.3-5 the diagonal elements of the variance-covariance matrix for case (3) are tabulated. The characteristics of this table are similar to those of Table 3.3-3 for case (1). From both tables it can be seen that

86

Table 3.3-4

Variances of Parameters for Case 2, (One Laser Station Observing,
Period of Observations Varied)

Parameters	50 Observations 3 Months	50 Observations 6 Months	50 Observations 9 Months	100 Observations 9 Months
	$meter^2$	$meter^2$	$meter^2$	$meter^2$
u	312	3.03	1.2	0.43
v	19.6	0.2	0.1	0.03
w	36.0	30.0	10.7	2.88
x_1	16.3	5.4	4.9	2.0
y_1	57.1	16.9	13.4	7.1
z_1	646.3	563.1	241.7	117.4
x_2	10.5	3.7	3.1	1.6
y_2	138.7	48.0	35.4	16.8
z_2	627.4	531.2	211.5	92.2
x_3	17.5	16.3	14.4	12.3
y_3	113.2	45.1	28.0	19.8
z_3	539.6	437.2	168.0	85.5
	$second^2$	$second^2$	$second^2$	$second^2$
δ_1	0.6×10^{-3}	0.3×10^{-3}	0.7×10^{-4}	0.2×10^{-4}
δ_2	0.3×10^{-2}	0.5×10^{-3}	0.7×10^{-3}	0.1×10^{-3}
δ_3	0.5	0.4×10^{-2}	0.2×10^{-2}	0.6×10^{-3}
τ	1.5	0.48	0.4	0.2
σ	397.8	392.4	372.2	348.5
ρ	1.4	1.38	1.2	1.0
C_{22}	0.3×10^{-2}	0.4×10^{-3}	0.2×10^{-3}	0.9×10^{-4}
β	0.4×10^{-3}	0.4×10^{-4}	0.3×10^{-4}	0.2×10^{-4}
C_{20}	0.1×10^{-3}	0.1×10^{-3}	0.1×10^{-3}	0.1×10^{-3}
	sec^2/day^2	sec^2/day^2	sec^2/day^2	sec^2/day^2
δ_4	0.2×10^{-2}	0.5×10^{-3}	0.1×10^{-2}	0.2×10^{-3}
δ_5	0.6×10^{-1}	0.2×10^{-1}	0.6×10^{-2}	0.8×10^{-3}
δ_6	0.4×10^{-3}	0.1×10^{-3}	0.4×10^{-4}	0.6×10^{-5}
$\dot{\tau}$	0.8×10^{-3}	0.1×10^{-3}	0.5×10^{-4}	0.2×10^{-4}
$\dot{\sigma}$	98.2	94.5	80.9	68.9
$\dot{\rho}$	0.02	0.015	0.014	0.013

Table 3.3-5

Variances of Parameters for Case 3 (Three Laser Stations Observing,
Number and Period of Observations Varied)

Parameters	50 Observations 3 Months	100 Observations 6 Months	150 Observations 9 Months	200 Observations 12 Months
	$meter^2$	$meter^2$	$meter^2$	$meter^2$
u_1	169.43	1.17	0.1	0.04
v_1	10.61	0.08	0.02	0.01
w_1	9.69	2.49	1.26	0.75
u_2	43.04	0.34	0.04	0.02
v_2	119.04	0.81	0.08	0.03
w_2	8.08	2.14	1.05	0.62
u_3	38.88	0.25	0.03	0.01
v_3	85.47	0.59	0.06	0.03
w_3	9.83	2.51	1.26	0.76
x_1	10.50	2.51	0.97	0.47
y_1	43.26	6.92	3.09	1.61
z_1	243.70	131.25	82.21	49.60
x_2	6.71	2.08	0.87	0.46
y_2	81.66	22.11	8.23	3.96
z_2	207.30	96.73	62.80	42.57
x_3	17.05	13.90	9.62	6.25
y_3	67.06	17.71	8.21	3.83
z_3	197.62	98.69	64.18	40.77
	$second^2$	$second^2$	$second^2$	$second^2$
δ_1	0.14×10^{-3}	0.38×10^{-4}	0.21×10^{-4}	0.15×10^{-5}
δ_2	0.11×10^{-3}	0.39×10^{-4}	0.23×10^{-4}	0.14×10^{-4}
δ_3	0.25	0.17×10^{-3}	0.15×10^{-3}	0.63×10^{-4}
τ	0.94	0.23	0.83×10^{-1}	0.39×10^{-1}
σ	397.58	378.84	335.64	247.27
ρ	1.44	1.14	0.76	0.44
C_{22}	0.17×10^{-2}	0.20×10^{-3}	0.38×10^{-4}	0.14×10^{-4}
β	0.48×10^{-3}	0.25×10^{-4}	0.80×10^{-5}	0.33×10^{-5}
C_{20}	0.1×10^{-3}	0.1×10^{-3}	0.1×10^{-3}	0.1×10^{-3}
	sec^2/day^2	sec^2/day^2	sec^2/day^2	sec^2/day^2
δ_4	0.50×10^{-3}	0.18×10^{-3}	0.12×10^{-3}	0.63×10^{-4}
δ_5	0.99×10^{-2}	0.18×10^{-2}	0.68×10^{-3}	0.23×10^{-3}
δ_3	0.67×10^{-4}	0.12×10^{-4}	0.46×10^{-5}	0.16×10^{-5}
$\dot{\tau}$	0.55×10^{-3}	0.55×10^{-4}	0.13×10^{-4}	0.53×10^{-5}
$\dot{\sigma}$	97.37	78.40	51.74	30.10
$\dot{\rho}$	0.16×10^{-1}	0.15×10^{-1}	0.13×10^{-1}	0.93×10^{-2}

the accuracy of determining the parameters naturally increases with an increase in the number of observations and the period of observations. The largest degree of improvement is obtained when the number and period of observations are increased from 50 and three months to 100 and six months respectively. The least sensitive parameters in the adjustment model remain the moon's physical libration in node and its time derivative (σ and $\dot{\sigma}$). No particular advantage is evident observing from three rather than from a single station except that, of course, more station coordinates can be determined.

The first striking feature of the correlation matrix (not presented here) is the high correlation that exists between the u and v coordinates of a given laser station as well as the high correlation between the x and y coordinates of the retroreflectors. The u coordinates are also correlated among one another, and the same applies to the v, w, x, y, z coordinates. These phenomena may be due to the fact that the orientation of both the earth and the moon as well as the geocenter are part of the parameters in the solution. It can also be noticed that there is a high correlation between δ_5 and δ_6, as well as between δ_2 and δ_4. For the lunar orientation parameters, high correlation exists between σ and ρ, and ρ and σ. Coordinates of laser stations seem to be correlated neither with the selenodetic coordinates of the reflectors nor with the orientation parameters of the moon.

4. CURRENT WORK

As can be seen from the previous sections several significant studies have been accomplished dealing with lunar feature positioning (selenodesy) relative to lunar/geodetic/celestial coordinate systems using optical data from the earth or orbiting satellites and laser ranging or radio interferometry [Fajemirokun, 1971; Papo, 1971]. The above reports have been criticized by other scientific investigators because of some of the simplistic assumptions made in the theoretical developments [LURE Team Conference, 1971; Kaula, 1972].

At present, "in situ" lunar exploration ended with the return of Apollo 17. However, the "new" types of data available for selenodesy and particularly the combination of available data types has barely begun. Government sponsorship (NASA) has created teams of highly competent scientists to analyze particular types of data. Thus we have a Lunar Laser Ranging Experiment (LURE) Team, a "Photographic" Team, etc. for various data types. A brief scan of the available literature from the diverse groups should convince any investigator of the need for amalgamation of data types which would be interesting and, perhaps, fundamental in future selenodetic studies.

Current and future work is therefore twofold in that it would (1) create a realistic mathematical earth-moon dynamical model which would be free from the criticism mentioned and (2) simulate the following data types for use in determining selenodetic control and tracking station geodetic control.

91

A. Lunar Ranging. This study would involve the use of laser ranging for selenodesy using a realistic observational sequence from existing and proposed earth stations to existing lunar reflectors.

B. Lunar Interferometry. Proposals have been made [LURE Team Conference, 1971; Martin and Wells, 1972] to use the "packages" deposited by the crew members of Apollo 15, 16 and 17 for interferometric observations to manned spacecraft tracking stations. This study will involve a simulated "observational sequence" of Apollo packages for selenodetic purposes.

C. Very Long Baseline Interferometry (VLBI) Observations. The VLBI observations offer an excellent means of determining the earth's orientation and distances between observing stations. The theoretical mathematical development of VLBI observations has been included in [Fajemirokun, 1971]; however, in the amalgamated simulation the VLBI observations will be treated as distance/orientation constraints.

D. Apollo "J" Mission Data. The "near moon" metric photography with stellar camera orientation and laser altimetry obtained from the Apollo "J" series missions (numbered 15-17) will be examined for selenodetic purposes in conjunction with the other data types mentioned above.

E. Lunar Occultations. From the above investigation of existing new observational systems, it is apparent that relationships between the celestial, ecliptic and earth-fixed coordinate systems be carefully defined. An observational system defining a directional

92

relationship between these systems are occultation observations; consequently, simulated observations will be included in the final model.

As far as the earth-moon dynamic model is concerned, the approach will be the following:

(1) The rotation of the earth will be modeled as described in section 2.1.

(2) The rotation of the moon will be modeled as described in [Papo, 1971] and section 2.2.

(3) The rotation of the moon about the earth (e.g., the lunar ephemeris requires further consideration. In previous reports the lunar ephemeris was assumed to be correct. Obviously, this is an incorrect assumption since the lunar ephemeris is one of the major "unknowns" in light of modern observational systems. In considering this problem we have considered the following factors:

A. The first system would be to use an existing analytical ephemeris expressing the coordinates of the moon as a function of time and partial derivatives of the coordinates as a function of time. The disadvantages of using an existing analytical theory are twofold. First, many hundreds of terms must be used to determine each coordinate; consequently, the technique is computationally unfeasable. Second, the lunar coordinates determined from analytical theory have been proven inadequate for analysis of high precision lunar observation systems.

B. The second and most widely used system by agencies analyzing real precise lunar data are numerically integrated ephemerides. In our previous

reports we used the Lunar Ephemeris (LE) number 16 contained in the Development Ephemeris (DE) number 69 created by the Jet Propulsion Laboratory (JPL). Subsequently, JPL has created other ephemerides based on the most recent observational evidence. The lunar coordinates available from numerically integrated ephemerides are the most accurate coordinates available. Unfortunately, however, differential corrections to parameters which were used in the theory are not available.

C. The third system and one used in previous reports is to create a simulated environment in which a simplistic mathematical formulation of the earth/moon/sun system and use numerical integration to create "simulated" lunar ephemerides with corresponding formulation to correct the ephemerides in an adjustment model. The difficulty with this approach is that it greatly oversimplifies the complex intercoupled lunar theory.

D. Finally, the most reasonable system to be used in future simulations is to first assure available accuracy for lunar coordinates by using a numerically integrated ephemeris and, second, to allow corrections to be formulated for the theory by using analytic partial derivatives of the coordinates with respect to the main elements of lunar theory.

5. BIBLIOGRAPHY

5.1 Interim Reports Prepared Under the Contract

The Ohio State University Department of Geodetic Science Reports:

127 A General Review and Discussion on Geodetic Control on the Moon
   by Ivan I. Mueller   December, 1969
          (Interim Report No. 1)

143 Establishment of Selenodetic Control Through Measurements on the
   Lunar Surface
   by Robert McLean   September, 1970
          (Interim Report No. 2)

144 An Investigation to Improve Selenodetic Control Through Surface
   and Orbital Lunar Photography
   by Harry Jauncey Sweet, III   September, 1970
          (Interim Report No. 3)

155 An Investigation to Improve Selenodetic Control on the Lunar Far
   Side Utilizing Apollo Mission Trans-Earth Trajectory Photography
   by Michael D. Sprague   June, 1971
          (Interim Report No. 4)

156 Optimal Selenodetic Control
   by Haim B. Papo   August, 1971
          (Interim Report No. 5)

157 Application of New Observational Systems for Selenodetic Control
   by Francis A. Fajemirokun   December, 1971
          (Interim Report No. 6)

176 An Investigation to Improve Selenodetic Control on the Lunar Limb
   Utilizing Apollo 15 Trans-Earth Photography
   by Wyndham Riotte   June, 1972
          (Interim Report No. 7)

197 Selenodetic Computer Programs
   by F.A. Fajemirokun, F.D. Hotter and H.B. Papo   February, 1973
          (Interim Report No. 8)

5.2 Other References

Alley, C.O. et al. (1970). "Laser Ranging Retroreflector: Continuing Measurements and Expected Results." Science, 167, pp. 458-460.

Brouwer, D. and G. Clemence. (1961). Methods of Celestial Mechanics. Academic Press, New York, p. 3.

Brown, E.W. (1908). "Theory of the Motion of the Moon." Memoirs of the Royal Astronomical Society, 59, pp. 1-103.

Eckert, W.J. et al. (1954). Improved Lunar Ephemeris 1952-1959. U.S. Naval Observatory.

Eckhardt, D.H. (1967). "Lunar Physical Libration Theory." Measure of the Moon, Kopal and Goudas (eds.). D. Reidel Publishing Co., Dordrecht, Holland.

Eckhardt, D.H. (1970). "Lunar Libration Tables." The Moon, 1, 2, February.

Edwards, Hiram W. (1964). Analytic and Vector Mechanics. Dover Publications Inc., New York.

Fajemirokun, F.A. (1971). "Applications of Laser Ranging and VLBI Observations for Selenodetic Control." Reports of the Department of Geodetic Science, 157, The Ohio State University, Columbus.

Kaula, W.H. (1972). "Potentialities of Lunar Laser Ranging for Measuring Tectonic Motions." Submitted to Philosophical Transactions of the Royal Society.

Kopal, Z. (1969). The Moon. D. Reidel Publishing Co., Dordrecht, Holland.

Krogh, Fred T. (1969). "VODQ/SVDQ/DVDQ - Variable Order Integrators for the Numerical Solution of Ordinary Differential Equations." Section 314, Subroutine Write-Up, Jet Propulsion Laboratory, Pasadena, Calif.

LURE Team Conference. (1971). Unpublished personal notes. Boulder, Colo.

Martin, C.F. and D.M. Wells. (1972). "Evaluation of Tracking Station Coordinates Using Metric Tracking Data." Paper No. G-25 submitted at the American Geophysical Union, Annual Fall Meeting, D.

Melbourne, W.G. et al. (1968). "Constants and Related Information for Astrodynamic Calculations, 1968." Technical Report 32-1306, Jet Propulsion Laboratory, Pasadena, Calif.

Mueller, Ivan I. (1969). Spherical and Practical Astronomy As Applied to Geodesy. Frederick Ungar Publishing Co., New York.

Mueller, Ivan I. (1969a). "A General Review and Discussion on Geodetic Control of the Moon." Reports of the Department of Geodetic Science, 127, The Ohio State University, Columbus.

96

O'Handley, D.A. et al. (1969). "JPL Development Ephemeris No. 69." Technical Report 32-1465, Jet Propulsion Laboratory, Pasadena, Calif.

Papo, Haim B. (1971). "Optimal Selenodetic Control." Reports of the Department of Geodetic Science, 156, The Ohio State University, Columbus.

Plummer, H.C. (1960). An Introductory Treatise on Dynamical Astronomy. Dover Publications Inc., New York.

Sprague, M.D. (1971). "An Investigation to Improve Selenodetic Control on the Lunar Far Side Utilizing Apollo Mission Trans-Earth Trajectory Photography." Reports of the Department of Geodetic Science, 155, The Ohio State University, Columbus.

Williams, J.G. (1973). Private communication.

Woolard, E.W. (1953). "Theory of the Rotation of the Earth Around Its Center of Mass." Astronomical Papers Prepared for the Use of the American Ephemeris and Nautical Almanac, XV, Part 1. U.S. Government Printing Office, Washington, D.C.